DESIGN AND OPTIMIZATION OF POWER SUPPLIES FOR WIRELESS INTEGRATED MICROSYSTEMS

by

Fabio Albano

A dissertation submitted in partial fulfillment
of the requirements for the degree of
Doctor of Philosophy
(Material Science and Engineering)
in The University of Michigan
2008

Doctoral Committee:

Professor Ann Marie Sastry, Chair
Professor Yogesh B. Gianchandani
Professor J. Wayne Jones
Professor Johannes W. Schwank

10 And the disciples came, and said unto him, Why speakest thou unto them in parables?

11 He answered and said unto them, Because it is given unto you to know the mysteries of the kingdom of heaven, but to them it is not given.

12 For whosoever hath, to him shall be given, and he shall have more abundance: but whosoever hath not, from him shall be taken away even that he hath.

13 Therefore speak I to them in parables: because they seeing see not; and hearing they hear not, neither do they understand.

14 And in them is fulfilled the prophecy of Esaias, which saith, By hearing ye shall hear, and shall not understand; and seeing ye shall see, and shall not perceive:

15 For this people's heart is waxed gross, and their ears are dull of hearing, and their eyes they have closed; lest at any time they should see with their eyes and hear with their ears, and should understand with their heart, and should be converted, and I should heal them.

16 But blessed are your eyes, for they see: and your ears, for they hear.

17 For verily I say unto you, That many prophets and righteous men have desired to see those things which ye see, and have not seen them; and to hear those things which ye hear, and have not heard them.

(Matthew 13:10-17)

In memory of my grandmother, Isabella Riso (1908-2002),
of my aunt Gianna Suraci (1940-1989) and
of my grandfather Giovanni Battista Suraci (1905-1995);
of my friends
Victoria Cafasso (1975-1995) and Rachel Persico (1953-2007)
and
to my parents Mario Albano and Domenica Suraci.

ACKNOWLEDGEMENTS

Firstly, and foremost, I would like to thank my advisor Prof. Ann Marie Sastry for her teachings and for offering me an opportunity of a lifetime. Her great expertise and knowledge of the Sciences and Engineering as well as the life in Academia inspired and made this work possible.

Thank you to my committee members — Prof. Yogesh B. Gianchandani, Prof. J. Wayne Jones and Prof. Johannes W. Schwank for your time and advice.

A big thank you to my friend and former colleague Prof. Kimberly Cook, for listening and being present, helping to get things done and for guidance and support through the graduate student life.

Dr. Chia-Wei Wang, a friend, colleague and future venture partner, thank you for always being encouraging, thoughtful and reassuring.

Also, I would like to thank my colleagues from Prof. Sastry's group, Dr. Munish Inamdar, Mr. Yen-Hung Chen, Mr. Hyon Cheol Kim, Mr. MyoungDo Chung, Mr. Xiangchung Zhang, Mr. Peter Verhees and Mr. Min Zhu for a great time and support throughout the last four years.

A special thank you to my best friend Mr. Robert Mitchell (Cyon Flare) for listening, being there when I needed it, providing an example of love and survival to follow and defy any fear.

A big thank you to Mr. Stefan Blumer, a friend and roommate, your jovial

attitude, keen spirit and love provided infinite support.

Mr. Fj Cava, a best friend and travel companion, for supporting me through difficulties and providing an example of strength and bravery by starting a venture in a remote and difficult country like Gabon (Africa).

Thank you to my friend Mr. James Sims III (Giacomo), for love and support and for showing me aspects of my own culture from an American perspective.

Dr. Daniela Brusaschetto, a best friend and travel companion, for listening and for supporting through her love all the way from Italy.

A special thank you to Ms. Tiziana Tinti, a partner, friend and confidant, your energy, love and advice provided a safe harbor to navigate through life.

Dr. Emiliano Spatti, my roommate from college and best friend from high school, the many memories we share have supported me all the way.

Mr. Fabio Trevisan, long term friend and buddy, for being always present with help and support.

Dr. Sigrun Karlsdottir, a friend and classmate, for providing an example of strength and for help and support through graduate school.

Thank you to my friend and graduate schoolmate Mr. Andrea Bianchini, for reminding me that Italians are excellent scientist and strong people and for helping and supporting.

Dr. Ferdinand Kappes, a fine scientist, friend and confidant, for reminding me to work hard but also to enjoy life and find time to party after work.

Prof. Eugene Bowen, a mathematician and best friend, for supporting me in my academic life and for listening and supporting in my private life.

Ms. Yiting (Tracy) Yu, a friend and travel companion, for reminding me of my strength, introducing me to her culture and for encouraging all the time.

Dr. Kahn Wu, for being a good friend and travel companion, for helping while we were students and challenging me while we were skiing.

Ferial and Jeff Rewoldt for their love and support during my student life in Ann Arbor.

Marcia and Greg Jablonski for their love and for spending time learning and speaking Italian.

Finally, and most importantly, I would like to thank all of my friends that were not named here and my parents Mario Albano and Domenica Suraci, for their endless love and support.

I would like to thank for support the WIMS-ERC, Engineering Research Centers program of the National Science Foundation under NSF Award Number EEC-9986866; the Assistant Secretary for Energy Efficiency and Renewable Energy, Office of FreedomCAR and Vehicle Technologies of the U.S. Department of Energy under contract No. DE-AC02-05CH11231, subcontract No. 6720903.

TABLE OF CONTENTS

LIST OF TABLES

LIST OF FIGURES

LIST OF ABBREVIATIONS

C	discharge rate [A]; C/5 is the current [A] to fully discharge a battery in 5 hours
CI	cochlear implant
CVD	chemical vapor deposition
DC	duty cycle
E^0	standard electrode potential [V]
EMT	Environmental Monitor Testbed
FDA	Food and Drug Administration
FEG	field emission gun
HIPS	Hybrid Implantable Power System
HPS	Hybrid Power System
IOS	Intra-Ocular Sensor
IOS-1	first battery prototype
IOS-2	second battery prototype
IOS-3	third battery prototype
IOS-C-1	first O~cm^2 battery prototype
IOS-C-2	second O~cm^2 battery prototype
IOS-C-3	third O~cm^2 battery prototype
IOS-M-1	first O~mm^2 battery prototype
IOS-M-2	second O~mm^2 battery prototype
IOS-X-1	on-chip battery prototype
IPS	Implantable Power System
MAV	micro air vehicle

MEMS	microelectromechanical systems
O~	Landau notation, O~cm^3 = order of cm^3
PDMS	polydimethylsiloxane
POWER	Power Optimization for Wireless Energy Requirements, a Matlab® algorithm.
PS	power supply
PVD	physical vapor deposition
SEI	Solid Electrolyte Interface
SEM	scanning electron microscope
TFB	thin film battery
WIMS-ERC	Wireless Integrated Micro- Systems – Engineering Research Center
XEDS	X-ray energy dispersive spectroscopy

ABSTRACT

In this work, we developed a novel power supply for the WIMS-ERC intraocular sensor (WIMS-IOS), an autonomous and implantable system. This device is representative of a broad class of microscale devices, whose full implementation in environmental and medical systems will require significantly smaller power supplies; presently, battery systems represent 85% mass and 50% volume of typical devices. Strategies using both commercial and specially developed devices, using a variety of electrochemistries have been used.

The smallest of the batteries reported to date, are thin-film lithium (Li) cells, using a chemical vapor deposition (CVD) or a pulsed laser deposition (PLD) approach. Thin film batteries fabricated with these techniques have achieved electrodes thicknesses less than 5μm (unpackaged), capacities of ~100μAh/cm^2 and footprints of 1cm^2. However, clean-room fabrication and high power laser equipment needed for ceramic materials entail high cost (~$300/Wh), and the elevated processing temperatures (500-720ºC) and use of chemicals and etchants, make them incompatible with CMOS materials. Finally, the intrinsically high power (3.5-4.2V) of lithium chemistry complicates integration with low-voltage MEMS, since it necessitates voltage regulation.

In our study we deposited thin film electrodes using physical vapor deposition (PVD), a low temperature (270-500ºC) purely physical process in a vacuum ~10^{-7}Torr. Our underlying hypothesis was that this technique would reduce intrinsic losses because

of the high resulting precision, while allowing integration with chips because of more benign processing conditions to MEMS. Our specific objectives were to: 1) analyze commercial systems for the WIMS-IOS; 2) create batteries from commercial active materials; and finally 3) create test and integrate novel batteries. Commercial Zn/Ag batteries were selected using a previously developed system analyzer (POWER algorithm). Active materials from the same commercial systems were packaged in ceramics and tested in three cells. Six novel cells (cathode/anode) were deposited on MEMS platforms (glass substrates). The last of these was integrated with the WIMS-IOS microchip and tested. Deposited batteries had suitable voltages (1.55) for MEMS, thicknesses of ~25μm (unpackaged) and footprints of ~2mm^2, with capacities ~0.1mAh/cm^2, and processing conditions compatible with MEMS materials. They also offer potentially lower cost than existing systems.

CHAPTER I

INTRODUCTION

MOTIVATION

The reduction in size of CMOS technology has triggered a higher number of components that could be accommodated inside MEMS (microelectromechanical systems) and consequently has introduced a proportional increase in power consumption and leakage [1]. Major obstacles remain in developing devices of very small scale (<1mm) [2], presently available battery cannot meet the increasingly small dimensions and growing power consumption of such devices [3]. The progress of mobile electronics will depend on the development of inexpensive, small and high capacity batteries [4]. At present the majority of portable and wireless electronic devices power supply relies on traditional rechargeable batteries (secondary cells), with Li-ion being the most widely used electrochemistry as reported in Table 1.1.

Continuous penetration of MEMS in the medical field has enabled implantable systems of sub-millimeter sizes [7], however batteries on the same scale of novel devices are not available. Hence further miniaturization and integration of implantable systems will require new battery technologies, compatible with MEMS (microelectromechanical systems) and of microscopic dimensions. To fulfill the increasing demand of miniature power sources, invention and commercialization of novel

storage devices like micro- fuel cells, micro- batteries and thin-film batteries are compelling needs and represent technological bottlenecks.

device	wireless power supply	power grid connection
cellphone	Li-ion cells (secondary)	• battery recharge • antennas • voice/data transfer
Laptop/PDA	Li-ion cells (secondary)	• battery recharge • internet access • e-mail, IM and data send/transfer
MP3 player/ gaming console	Li-ion cells (secondary)	• battery recharge • data transfer
digital camera	primary or secondary cells	• battery recharge • pictures send/transfer
wireless LAN	secondary cells (laptop)	• permanent connection to power antenna • battery recharge

Table 1.1. Wireless communication storage technologies [2, 3, 5, 6].

Traditional Zn-air, Li metal, Li-ion or Zn/AgO batteries, with costs ranging from 0.5 to 2.5$/Wh [8] have been utilized to power MEMS because of the lack of *ad-hoc* power sources. Even if thin film batteries (TFBs), due to their excellent energy density, have been investigated for powering such applications at present they require large surface areas to output sufficient capacity, preventing their practical utilization. Currently there are essentially no thin film batteries that have a surface area smaller than 1cm^2, that

could achieve capacities higher than 100μAh, or that could have lifetimes longer than a day without carrying prohibitive costs (~$300/Wh [9]). Size reduction and increase in electrodes capacity (3D electrodes) have scaled with manufacturing costs of batteries, due to the application of techniques typical for microchip fabrication (photolithography, masking, etching) and to low production volumes.

BACKGROUND

Presently, 620 million cellphones, 75 million camera phones, 50 million digital cameras and 11.5 million PDAs are sold worldwide every calendar year [10, 11]. Consumer wireless communications and networking are used for voice, messaging (email, instant messages, short text messages), domestic data transmission, Internet services, home automation and sensing, entertainment, toys and games, meter reading and biomedical applications. Wireless and autonomous MEMS devices used in environmental [12] biological [13, 14] and medical [15, 16, 17] applications rely mainly on batteries for power. Because power sources on the same scale of the devices cannot be found, in all the examples above the power supplies comprise up to 80% the mass and 50% volume of the system.

Considerable work has been performed to achieve miniaturized power sources, independent of specific applications. Li-ion microbatteries [18, 19, 20, 21, 22, 23] have been widely investigated because of their high nominal voltage (~3.7V), giving them a much higher capacity than other electrochemistries, e.g. Ni/Zn (~1.8V) [24, 25, 26] or Ag/Zn (~1.55V). Very low thicknesses, ranging from ~15μm (Li-ion) to ~100μm (Li-ion, Ni/Zn, Ag/Zn) have been achieved; however microelectronics and MEMS applications, requiring high capacity (up to 20mAh/cm^2 [3]), cannot presently be powered by such

intrinsically low capacity technologies. Though power densities as high as 30-70mW/cm^2 have been achieved by microbatteries, their low capacity (maximum ~100μAh/cm^2 achieved in commercial TFBs [27]) remains a major limitation. More recently, 3D electrode architectures have demonstrated increased specific capacities (e.g. 3.5mAh/cm^2 [28], and 500mAh/g [29]) allowing use of batteries with greatly reduced surface areas.

Selection of a power source relies on more than simply the electrochemistry. Form factor, performance, lifetime, toxicity of the chemicals and the rate of heat generation from the battery must be weighed, particularly in implantable systems.

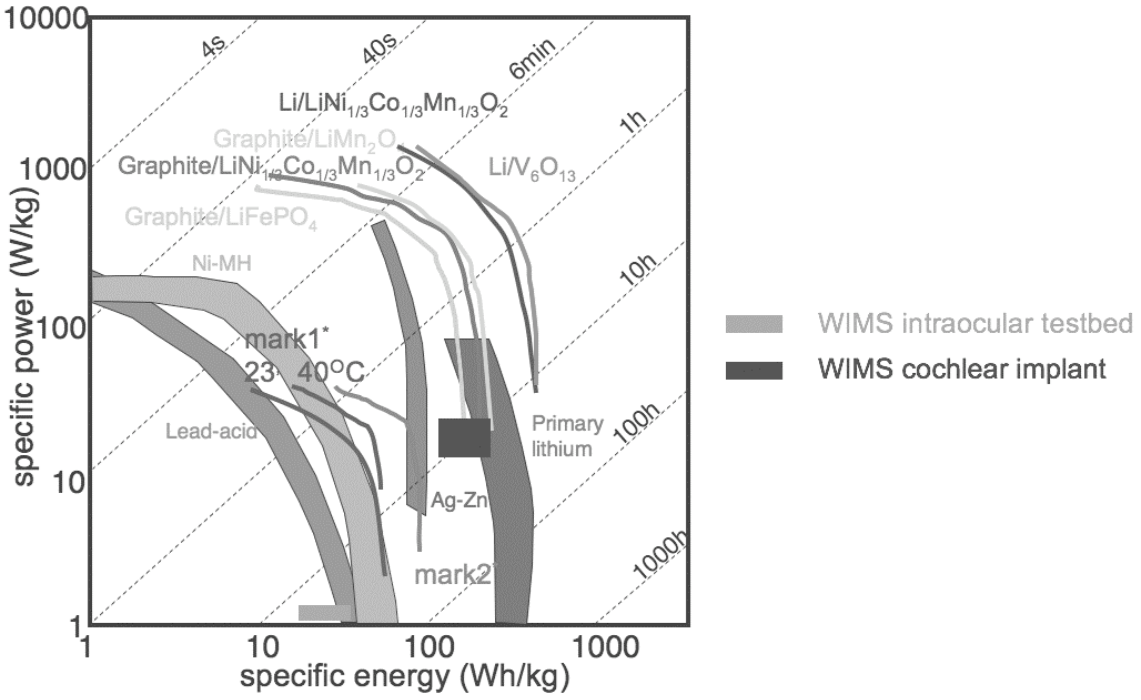

Figure 1.1. Ragone plot of primary and secondary batteries compared to WIMS goals. [30, 31, 32].

In Figure 1.1, we report a summary of gravimetric energy and power, for most commonly used electrochemistries and novel thin film batteries (Ragone plot). The Wireless Integrated Micro Systems – Engineering Research Center (WIMS-ERC) has developed very low power consumption chips [33, 34], defining the lower boundary in the MEMS power consumption domain. Even though current MEMS energy targets can be reached by a particular electrochemistry, all of the factors named above play a key role in selecting the winning electrochemistry for a certain application.

Dual battery systems to address variable rates of discharge have been developed and demonstrated by other groups to be effective in addressing this issue for portable electronics [35] and for select, implantable systems [36]. However, a method for development of a hybrid implantable power system (HIPS) that globally addresses all key constraints (lifetime, mass, volume, variable current draw etc.) has never been proposed prior to the present work.

Systems requiring complicated power profiles (e.g. high pulses, spikes or steady plateaus) or comprising subcomponent devices (e.g. the electrode array in the WIMS-CI [37] and the heating column in the WIMS-EMT [38]), provide an opportunity for hybridization of power supplies [39], comprising of more than one cell and/or electrochemistry. The WIMS-ERC intra-ocular sensor (IOS), an implantable microsystem of sub-millimeter size (~0.4mm^3 volume), implanted inside the eye to monitor glaucoma patients' intraocular pressure during treatment (≤2 years). This device presents an ultra low power consumption profile (O~pW) that makes it suitable for battery power design. The device is in "sleep" mode for almost 99% of the duty cycle with 1% "active" sensing periods of 30-50milliseconds during which the power consumption never exceeds 1mW.

Even if the CMOS technology used to design the device allows a fully implantable sensor of very reduced size (~2mm^2), the power source is still a major contributor to device mass and volume and a missing component to realize a totally implantable sensor.

ORGANIZATION OF THE DISSERTATION

Chapter II details the design of an optimized power source for the WIMS intraocular sensor by applying the strategy demonstrated in the POWER algorithm [37, 38]. For this case study the algorithm database included thin film batteries and Ni or Ag electrochemistries. Remanufacturing of selected Zn/AgO commercial systems to reduce the battery size for the three prototypes.

Chapter III provides the details of a novel fabrication technique compatible with CMOS processes to manufacture microbatteries of the same scale of other MEMS components. Electrochemistry selection and experimental techniques are presented. Five microbattery prototypes, produced using the novel manufacturing technique, were tested and a fully integrated device (microsystem) was demonstrated using a sixth prototype as power source.

Chapter IV, to conclude, summarizes the major findings and future directions of our research.

BIBLIOGRAPHY

1. Chakraborty, R.S., Narasimhan, S. and Bhunia, S., "Hybridization of CMOS with CNT-Based nano-electromechanical switch for low leakage and robust circuit design," Ieee Transactions on Circuits and Systems I-Regular Papers, 2007. 54 (11): p. 2480-2488.

2. Simunic, T., Benini, L., De Micheli, G., "Energy-efficient design of battery-powered embedded systems," IEEE Transactions On Very Large Scale Integration (VLSI) Systems, 2001. 9: p. 15-28.

3. Long, J.W., Dunn, B., Rolison, D.R. and White, H.S., "Three-dimensional battery architectures," Chemical Reviews, (2004). 104 (10): p. 4463-4492.

4. Hanson, S., Zhai, B., Bernstein, K., Blaauw, D., Bryant, A., Chang, L., Das, K.K., Haensch, W., Nowak, E.J. and Sylvester, D.M., "Ultralow-voltage, minimum-energy CMOS," Ibm Journal Of Research And Development, 2006. 50 (4-5): p. 469-490.

5. http://www.capv.com/home/Press/itPress/2002/8.21.02, accessed 08/04/2005.

6. http://www.alexanderresources.com/reports/Report%2031/Summary.htm, accessed 08/04/2005.

7. Wise, K.D., "Silicon microsystems for neuroscience and neural prostheses," IEEE Engineering in Medicine and Biology Magazine, 2005. 24 (5), Sep-Oct: p. 22-29.

8. http://www.plasticlabels.ca/index_files/compareEVbatteries.htm, accessed 12/14/2007.

9. http://www.infinitepowersolutions.com, accessed 06/02/07.

10. http://www.insidedsp.com/Articles/tabid/64/articleType/ArticleView/articleId/113/Inside-DSP-on-Low-Power-Long-Live-the-Battery.aspx, accessed 01/13/2008.

11. http://insidedsp.eetimes.com/features/printableArticle.jhtml?articleID=21100222, accessed 08/04/2005.

12. Sato, H., Berry, C.W., Casey, B.E., Lavella, G., Yao, Y., Maharbiz, M.M., "A Cyborg beetle: insect flight control through an implantable, tetherless microsystem," accepted 21st IEEE International Conference on Micro Electro Mechanical System, 2008.

13. Lemmerhirt D.F. and Wise, K.D., "Chip-Scale Integration of Data-Gathering Microsystems," Proceedings of the IEEE, 2006. 94 (6): p. 1138-1159.

14. Mohseni, P., Najafi, K., Eliades, S.J. and Wang, X.Q., "Wireless multichannel biopotential recording using an integrated FM telemetry circuit," IEEE Transactions on Neural Systems and Rehabilitation Engineering, 2005. 13 (3): p. 263-271.

15. Nieder, A., "Miniature stereo radio transmitter for simultaneous recording of multiple single-neuron signals from behaving owls," Journal of Neuroscience Methods, 2000. 101 (2): p. 157-164.

16. Johannessen, E.A., Wang, L., Cui, L., Tang, T.B., Ahmadian, M., Astaras, A., Reid, S.W.J., Murray, A.F., Flynn, B.W., Beaumont, S.P., Cumming, D.R.S. and Cooper, J.M., "Implementation of multichannel sensors for remote biomedical measurements in a microsystems format," IEEE Transactions on Biomedical Engineering, 2004. 51 (3): p. 525-535.

17. Obeid, I., Nicolelis, M.A.L. and Wolf, P.D., "A multichannel telemetry system for single unit neural recordings," Journal of Neuroscience Methods, 2004. 133 (1-2): p. 33-38.

18. Bates, J.B., Dudney, N.J., Neudecker, B., Ueda, A., and Evans, C.D., "Thin-film lithium and lithium-ion batteries," Solid State Ionics, 2000. 135 (1-4): p. 33.

19. Bates, J.B., Dudney, N.J., Neudecker, B.J., Hart, F.X., Jun, H.P. and Hackney, S.A., "Preferred orientation of polycrystalline $LiCoO_2$ films," Journal Of The Electrochemical Society, 2000. 147 (1): p. 59.

20. Neudecker, B.J., Dudney, N.J. and Bates, J.B., ""Lithium-free" thin-film battery with in situ plated Li anode," Journal Of The Electrochemical Society, 2000. 147 (2): p. 517.

21. Neudecker, B.J., Zuhr, R.A. and Bates, J.B., "Lithium silicon tin oxynitride (LiySiTON): high-performance anode in thin-film lithium-ion batteries for microelectronics," Journal Of Power Sources, 1999. 82: p. 27.

22. Dudney N.J. and Neudecker, B.J., "Solid state thin-film lithium battery systems," Current Opinion In Solid State & Materials Science, 1999. 4 (5): p. 479.

23. Bates, J.B., Dudney, N.J., Lubben, D.C., Gruzalski, G.R., Kwak, B.S., Yu, X.H. and Zuhr, R.A., "Thin-Film Rechargeable Lithium Batteries," Journal Of Power Sources, 1995. 54 (1): p. 58-62.

24. Humble, P.H., Harb, J.N. and LaFollette, R.M., "Microscopic nickel-zinc batteries for use in autonomous Microsystems," Journal Of The Electrochemical Society, 2001. 148 (12): p. A1357.

25. Harb, J.N., LaFollette, R.M., Selfridge, R.H. and Howell, L.L., "Microbatteries for self-sustained hybrid micropower supplies," Journal Of Power Sources, 2002. 104 (1): p. 46.

26. LaFollette, R.M., Harb, J.N. and Humble, P., in Sixteenth Annual Battery Conference On Applications And Advances, 2001, p. 349.

27. http://www.infinitepowersolutions.com, accessed 06/02/07.

28. Golodnitsky, D., Yufit, V., Nathan, M., Shechtman, I., Ripenbein, T., Strauss, E., Menkin, S. and Peled, E., "Advanced materials for the 3D microbattery," Journal of Power Sources, 2006. 153 (2): p. 281-287.

29. Wang, C.L., Taherabadi, L., Jia, G.Y., Madou, M., Yeh, Y.T. and Dunn, B., "C-MEMS for the manufacture of 3D microbatteries," Electrochemical and Solid State Letters, 2004. 7 (11): p. A435-A438.

30. http://www.corrosion-doctors.org/Batteries/images/Fig6rago.gif, accessed 01/14/2008.

31. http://berc.lbl.gov/venkat/lithium.html, accessed 01/14/2008.

32. Brandt, K., "Practical batteries based on the SWING system," Journal of Power Sources, 1995. 54: p. 151-154.

33. Seok, M., Hanson, S., Lin, Y.-S., Foo, Z., Kim, D., Lee, Y., Liu, N., Sylvester, D.M. and Blaauw, D., "The Phoenix Processor: A 30pW Platform for Sensor Applications," accepted IEEE International Solid State Circuits Conference, 2008.

34. Lin, Y.-S., Hanson, S., Albano, F., Tokunaga, C., Haque, R.-U., Wise, K.D., Sastry, A.M., Blaauw, D. and Sylvester, D.M., "Low-Voltage Circuit Design for Widespread Sensing Applications," accepted IEEE International Symposium on Circuits and Systems, 2008.

35. Wu, Q., Qiu, Q., Pedram, M., "An Interleaved Dual-Battery Power Supply for Battery-Operated Electronics," in IEEE (Ed.), Asia and South Pacific Design Automation Conference, Yokohama, Japan, 2000. p. 387-390.

36. Drews, J., Wolf, R., Fehrmann, G., Staub, R., "Development of a hybrid battery system for an implantable biomedical device, especially a defibrillator cardioverter (ICD)," Journal Of Power Sources, 1999. 80: p. 107-111.

37. Cook, K.A., Albano, F., Nevius, P.E. and Sastry, A.M., "POWER (power optimization for wireless energy requirements): A MATLAB based algorithm for design of hybrid energy systems," Journal Of Power Sources, 2006. 159, (1): p. 758-780.

38. Cook K.A. and Sastry, A.M., “An algorithm for selection and design of hybrid power supplies for MEMS with a case study of a micro-gas chromatograph system,” Journal Of Power Sources, 2005. 140 (1): p. 181-202.

39. Albano, F., Chung, M.D., Blaauw, D., Sylvester, D.M., Wise K.D. and Sastry, A.M., "Design of a Power Supply for an Intraocular Sensor, Using POWER (Power Optimization for Wireless Energy Requirements)," Journal of Power Sources, 2007. 170 (1): 216-224.

CHAPTER II

DESIGN OF AN IMPLANTABLE POWER SUPPLY FOR AN INTRAOCULAR SENSOR, USING POWER (POWER OPTIMIZATION FOR WIRELESS ENERGY REQUIREMENTS)[1]

INTRODUCTION

The reduction in size and power usage of MEMS (microelectromechanical systems) devices has enabled development of fully implantable medical devices [1], though major obstacles remain in developing devices of very small scale (<1mm) [2]. Power systems typically comprise ~85% mass and ~35% volume of these devices, with typical representative applications shown in Table 2.1 [3,4,5,6,7,8,9]. The smallest commercial batteries currently available on the market, with sizes that span the mm range, comprise Zinc and Lithium based electrochemistries (Zn-air, Zn/AgO, Li-polymer, Li/MnO_2, etc.). A stainless steel case is typically employed to contain the fluid electrolyte KOH (aq) or the gaseous reaction byproducts. The volume fraction of the case can represent up to 50%, a particularly onerous requirement for implantable technologies.

Further miniaturization of implantable systems will require new battery technologies, compatible with MEMS (microelectromechanical systems) fabrication techniques. One of the most challenging applications, an intraocular sensor (IOS)

[1] Material in this chapter is a published paper: F. Albano, M. D. Chung, D. Blaauw, D. M. Sylvester, K. D. Wise, and A. M. Sastry, "Design of an implantable power supply for an intraocular sensor, using POWER (power optimization for wireless energy requirements)," *Journal of Power Sources* **170**, (1), 216-224 (2007).

developed by the Wireless Integrated Micro-Systems – Engineering Research Center (WIMS-ERC) at The University of Michigan, is the subject of the present study. This device has power consumption of O~nW, drawing a current of O~nA, and other characteristics shown in Table 2.2.

operating voltage	350mV
current draw	12nA
power	4.2nW
available surface for power	1.28mm^2 (800x1600μm^2)
available volume for power	0.256mm^3 (800x1600x200μm^3)

Table 2.1. WIMS-ERC IOS specifications.

application	electrochemistry	clinical test	location	year
pacemaker	zinc-mercury	dogs and humans	USA	1958-1959
biotelemeter (monitoring device)	nickel-cadmium	dogs	USA	1982
MEI (middle ear implant)	primary MnO_2/Li secondary Ni-Cd	humans	JAPAN	1988
ventricular assist device, artificial heart	Li-ion	calves, pigs, human cadavers	USA	1995
TICA (hearing prosthesis)	secondary Ni-Cd	cats, dogs, humans	GERMANY	1998
spinal cord OFS (oscillatory field stimulator)	secondary Li-polymer	rodents, dogs, humans	USA	2005

Table 2.2. Evolution of implantable batteries, and clinical trials [4,5,6,7,8,9].

Indeed, this and other novel implantable biosensors, represent a huge change in the domain of required power for implantable power systems (IPS). The first of these, pacemakers, were developed in the U.S. in the late 1950s [4]. A primary battery, of ~ 30cm^3 in volume and with a 2-year lifetime, was implanted in a stainless steel case. The chest cavity provided sufficient volume for the installation of the large power source. As secondary cell technology appeared in the 1980s, with the introduction Ni-Cd rechargeable batteries, IPS of smaller volume were produced (O~10cm^3). Coupled with novel electronics technologies, these new power sources enabled development of auditory prostheses [6,8] that could fit within the relatively small volumes available in the human skull. More recent improvements in safety of the Li-ion technology, one of the most energy-dense electrochemistries, have made it a suitable candidate for medical implants. In 2005 a battery of approximately 5cm^3 was utilized to power a fully implantable spine stimulator [9].

Selection of a power sources relies on more than simply the electrochemistry. Form factor, performance, lifetime, toxicity of the chemicals and the rate of heat generation from the battery must be weighed, particularly in implantable systems. Recently, we have demonstrated a methodology for generating hybrid implantable power systems (HIPS), resulting in increased lifetime and decreased mass and volume (key parameters for implantation) [10,11]. Dual battery systems to address variable rates of discharge have been developed and demonstrated by other groups to be effective in addressing this issue for portable electronics [12] and for select, implantable systems [13].

However, a method for development of a hybrid implantable power system (HIPS) that globally addresses all key constraints (lifetime, mass, volume, variable current draw etc.) has never been proposed, to the authors' knowledge. Thus, the goals of this work are to do so, using the WIMS-ERC intraocular sensor (IOS) as a challenge problem (Fig. 2.1). Our specific objectives are fourfold:

1) To model the power usage of an intraocular sensor (IOS);

2) To develop a methodology for optimization of HIPS;

3) To apply the selection tool to identify candidate power systems; and

4) To establish a methodology to fabricate and test the performance of optimized anode and cathode couple.

Packaging optimization is reserved for future work. Our work spanned experimental and theoretical efforts, described in the next section.

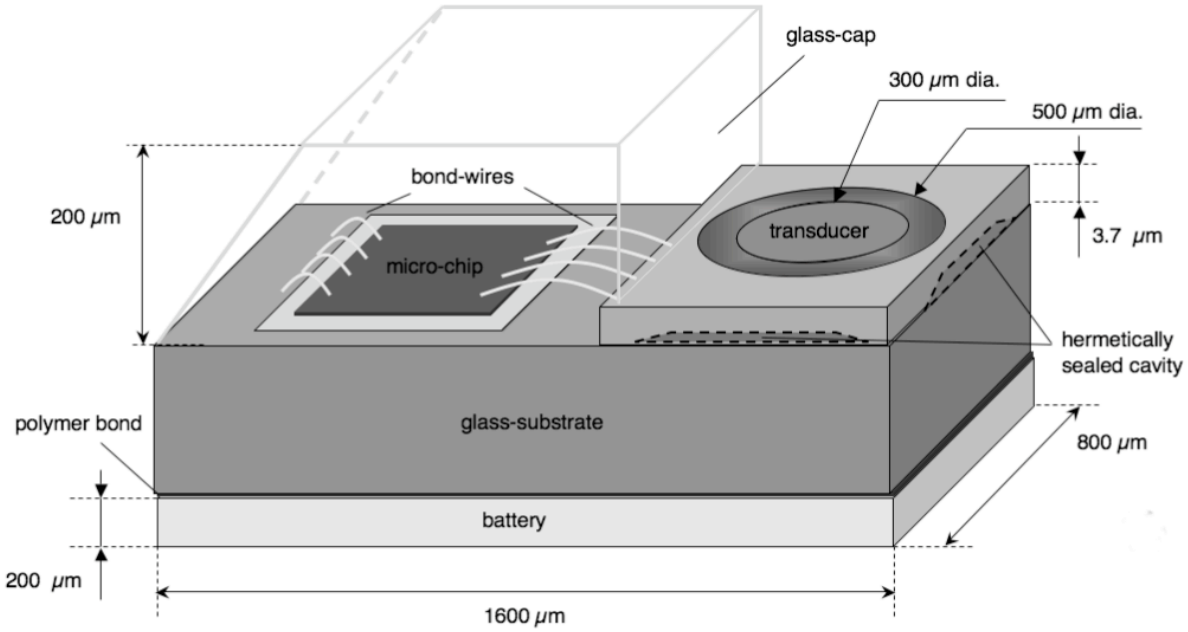

Figure 2.1. Schematic of WIMS-ERC IOS [27].

METHODS

In order to meet clinical goals, an IOS must be implanted within the eye, and continuously monitor pressure, for the entire period of treatment of a patient suffering from glaucoma. Treatment times vary, but are at most two years. During this time, a power supply is subject to a constant voltage and a constant current draw.

We utilized our code POWER to select the most suitable electrochemistry/ies and to determine the best cell configuration for this application. The input values for the code are reported in Table 2.3. To have a conservative evaluation we introduced a current draw for the optimization code around three orders of magnitude (10^3) higher than the one specified by the WIMS-ERC for this application.

The power profile of an IOS was determined by considering the device current draw specified by the WIMS-ERC and by coupling it with a patient daily routine. The device draws a constant current of approximately 12.0nA when activated, and a negligible current when kept in a sleep mode (~1nA). We estimated the active portion of the duty cycle to be 16 hours.

operating voltage [mV]	350mV
current draw [μA]	15μA
electrochemistry [primary/secondary]	primary
Prioritization [mass/volume]	mass
number of power sites	2
operation time [h]	16h

Table 2.3. Input parameters for POWER.

Once our code selected a suitable electrochemistry, theoretical values for voltage and capacity from the chemical reactions were calculated. Because these values can be significantly higher than practically achievable values, appropriate correction factors were included (typically 40% of the theoretical value is the actual capacity [14]). Calculated voltage and capacity were used to help identify candidate materials, and to estimate lifetime.

We proposed fabrication of a microbattery utilizing zinc and silver as electrode materials. Our battery database was adapted for the IOS case study by including cells with a flat discharge profile suitable for this kind of power draw, particularly Zn/AgO. For comparative purposes, a Ni/Zn secondary cell from Bipolar Technologies [15,16] was also added to our database to be employed as a primary cell. A comparison of these two electrochemistries is given in Table 6. Because of the rather short lifetime required by this application ($\leq$ 2 years), rechargeability was not taken into account in the POWER computation of the number of operation cycles provided by the battery. We investigated rechargeability of the batteries during our experimental evaluation, however, for the purpose of having different prototypes of batteries; we further felt it demonstrated system robustness.

We used POWER to identify suitable candidate commercial batteries. The version of the database used in this study comprised 194 primary batteries, including Zn/AgO, Ni/Zn, Zn/MnO_2, Alkaline, Lithium and Li/MnO_2 electrochemistries. The primary constraints were the size and shape (volume and form factor) and mass of the batteries. The secondary constraint was the implantability of the system. Electrochemistries that

have been previously tested in mammals and humans clinical studies (Table 2.2) were targeted.

In the present study we fabricated and tested three different cells, which we will refer to as IOS-1, IOS-2 and IOS-3 throughout the paper. The first battery, IOS-1, was designed to establish that a completely functional battery could be fabricated and sealed, starting from a commercial system. The second battery, IOS-2, was fabricated to investigate the effects of electrolyte fill inside the reaction chamber, and to determine if the cell could be recharged. The third battery, IOS-3, was designed to asses the effects of scaling down the battery system to the submillimeter size required by the application.

Battery IOS-1 was produced by resizing a Renata 317 Zinc/Silver oxide coin cell. The original cell has a diameter of 7.60mm and a thickness of 1.56mm. Using a Dremel® tool we removed the outer stainless steel case of the original cell. Anode, cathode, separator and sealing ring were collected. Current collectors were cut from a tin (Sn) foil into a shape suitable to contain the anode and cathode, and for connection of leads. Macor® ceramic (see Table 2.4 for chemical composition [17]) was utilized as material for building the battery package. Several battery half-packages were used, which had been fabricated from a 3.0 x 3.0in^2 tile of Macor® ceramic. Two round half-packages of inner diameter ~2.5mm and outer diameter ~4.5mm, with masses of ~0.05g each, were selected, among the previously produced samples, to hold anode and cathode materials, respectively. The electrodes were resized to fit an approximate area of ~4.9mm^2 (corresponding to a half package footprint) and a polypropylene separator membrane (DuPont® spunbonded polypropylene [18]) measuring ~4.0mm^2 was dissected.

Compound	Approximate Weight %
Silicon – SiO_2	46%
Magnesium – MgO	17%
Aluminium – Al_2O_3	16%
Potassium – K_2O	10%
Boron – B_2O_3	7%
Fluorine – F	4%

Table 2.4. Macor® ceramic composition [17].

The battery was then assembled. The first half-package was filled, with a current collector (Sn), the cathode material (AgO) and the polypropylene separator membrane (DuPont® spunbonded polypropylene [18]). The second half-package was filled, with a current collector (Sn) and the anode material (Zn). The two half packages were then flooded with the electrolyte, a solution of potassium hydroxide (28% KOH, 1% Li, from Yardney Technical Products Inc.). Using two parts epoxy resin (Emerson & Cuming type Stycast 2850FT black [19]), the package was sealed immediately, and was set to cure into a Plexiglass clamp for 24 hours. Rubber (PDMS) pads were used to distribute the load on the package and prevent cracking. Masses of active materials were not measured for this first cell, and thus theoretical capacity estimates were made after the package was sealed based on the approximate battery volume of 4.9mm^3. Once the battery was sealed, it was discharged at a constant load of ~11MΩ. The discharge current was measured using a Keithley current meter type 6517A. The discharge setup is described by the schematic on Fig. 2.2; data were collected using a National Instruments acquisition card type 6035E.

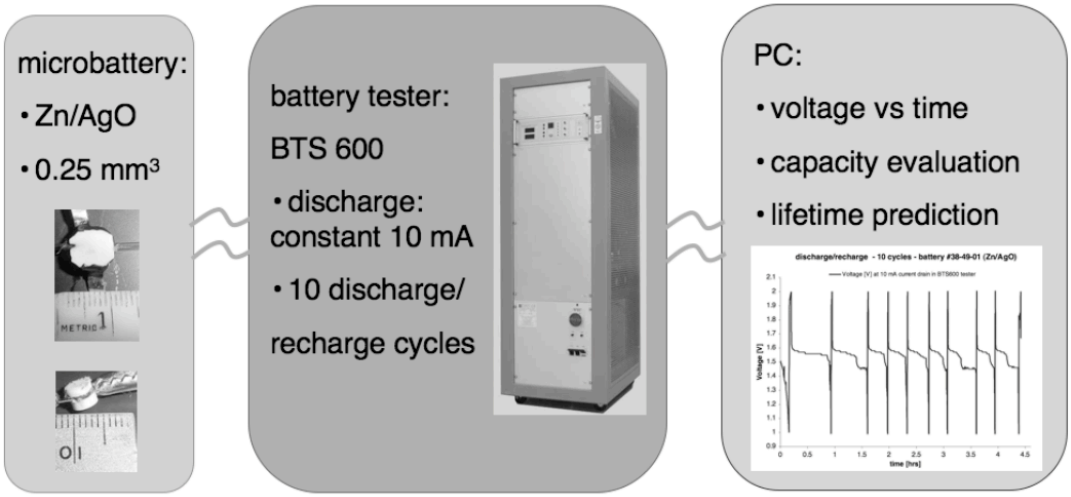

Figure 2.2. Schematic of the battery discharge setup.

Battery IOS-2 was produced using two cells type Renata 317, and tested according to the same procedure. A package was prepared by machining two pieces of Macor® ceramic Figs. 2.3a and 2.3b detail its geometry. Inlet and outlet channels were built into the package using a glass microtube, type μTIP™ - TIP5TW1 from WPI, as shown in Fig. 2.4. The mass of active material was recorded, and used to estimate theoretical capacity. The first half-package was filled with a current collector (Sn), 0.069g of the cathode material (AgO), and polypropylene separator membrane (DuPont® spunbonded polypropylene [18]). The second half-package was filled with a current collector (Sn), and 0.026g of anode material (Zn). Using two parts epoxy resin, Stycast 2850FT black, the package was sealed and cured in a Plexiglass clamp for 24 hours. No electrolyte was inserted into the package, and air was able to flow through the glass tubes. After the package was fully cured, electrolyte (28% KOH, 1% Li, from Yardney Technical Products Inc.) was inserted using an Eppendorf EZ-pet automatic pipette as a pumping device.

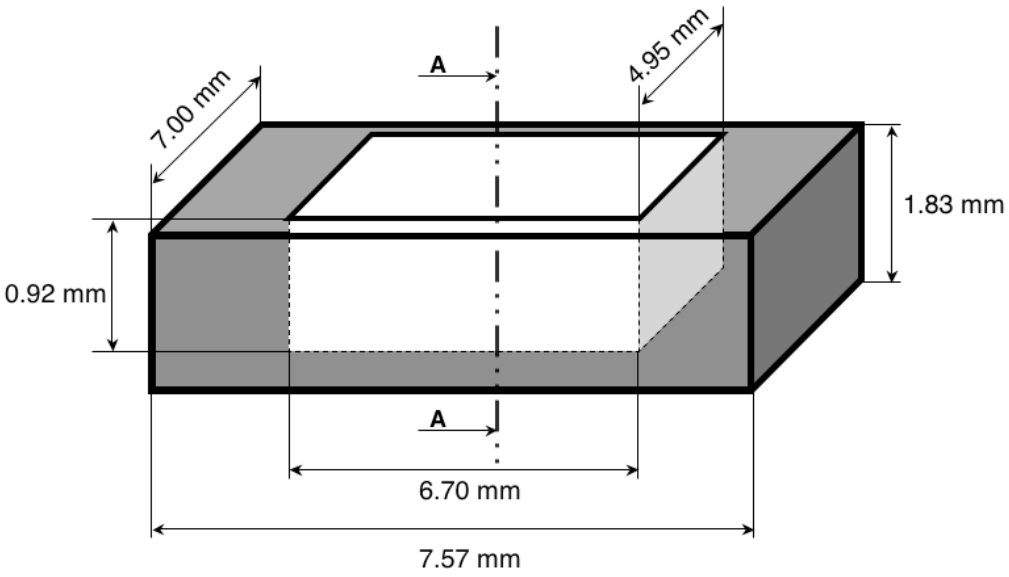

Figure 2.3a. Dimensions of IOS-2 package.

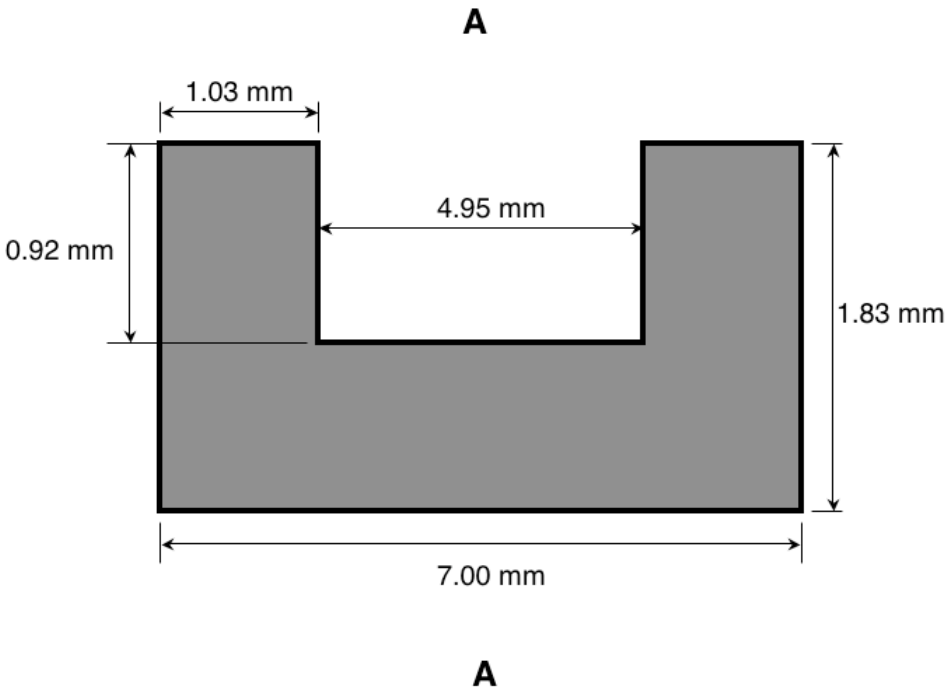

Figure 2.3b. Dimensions of IOS-2 package (section A-A).

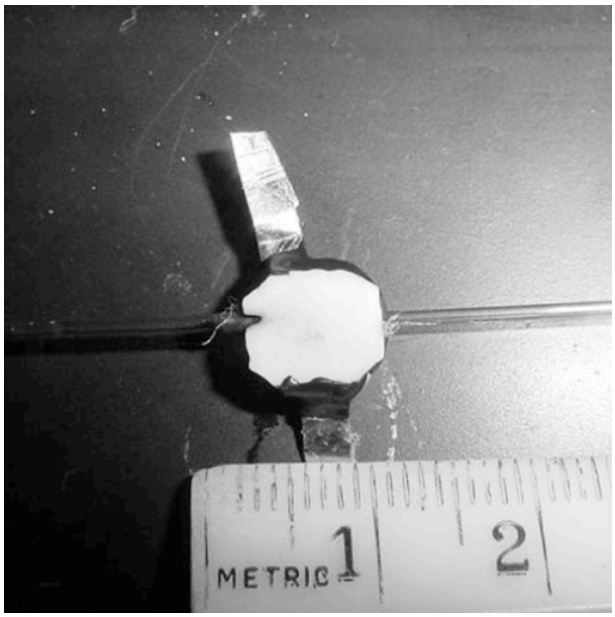

Figure 2.4. IOS-2, showing inlet and outlet glass tubes.

After ~3cc of electrolyte were allowed to flow through the battery using the pipette, the inlet and outlet channels were closed using PDMS stoppers. The battery was then discharged and the voltage was recorded. Once the voltage initially dropped below 1.1V, additional electrolyte was pumped into the battery under discharge, using the automatic pipette. After the voltage dropped a second time below 1.1V, the battery was disconnected and additional electrolyte was inserted. After this operation, voltage was recorded and the battery was cycled for 10 discharge/recharge cycles using a Firing Circuits battery tester type BTS600. The discharge voltage lower limit was set to 1.0V and the recharge voltage limit was set to 2.0V.

Battery IOS-3 was produced using another Renata 317 cell, and tested as before. The mass of active material was recorded, and used to estimate theoretical capacity. For this cell, current collectors were cut from a copper (Cu) foil. Two round Macor® ceramic packages of inner diameter ~1.5mm and outer diameter ~4.5mm, with masses of ~ 0.05g

each, were used for the external structure. The first half-package was filled with a current collector (Cu), 0.0040g of the cathode material (AgO), and polypropylene separator membrane (DuPont® spunbonded polypropylene [18]). The second half-package was filled with current collector (Cu) and anode material (Zn) in the amount of 0.0060g. The battery was again discharged according to the same procedure.

RESULTS

In Table 2.5 we report the results of our optimization routine (POWER). All three approaches selected a Zn/AgO commercial system from the database. Approach 1 selected a battery type Renata #364, with a mass of 0.32g and a volume of ~ 78.0mm^3. Approach 2 provided only one solution in the micro-power range (μW), selecting a battery type Maxell #SR421SW having a mass of 0.17g and a volume ~ 39.0mm^3. Approach 3 selected a battery type Renata #337 for each one of the two specified power sites presenting a mass of 0.12g and a volume of ~30.0mm^3. The resulting projected lifetimes of all three approaches exceeded the targeted lifetime (2 years), by more than three orders of magnitude.

WIMS-ERC - IO testbed - mass priority - 16 hours of operation							
	Manufacturer	Part No.	electro-chemistry	Total No.	No. of Cycles (no battery re-charge)	Total Mass [g]	Total Volume [cm^3]
Approach 1	Renata	364	Zn/AgO	1	2.21E+06	**3.20E-01**	7.81E-02
Approach 2							
micro	Maxell	SR421SW	Zn/AgO	1	2.13E+07	1.70E-01	3.89E-02
TOTALS				1	2.13E+07	**1.70E-01**	3.89E-02
Approach 3							
site 1	Renata	337	Zn/AgO	1	2.99E+04	1.20E-01	2.99E-02
site 2	Renata	337	Zn/AgO	1	2.99E+04	1.20E-01	2.99E-02
TOTALS				2		**2.40E-01**	5.98E-02

Table 2.5. Results of POWER analysis.

With the specified power requirements and volume constraints (Table 2.1) a nickel electrochemistry provides a lifetime of 0.64 years (~40% of theoretical, per [14]) not accounting for rechargeability, while a silver electrochemistry provides a lifetime of 3.63 years (~40% of theoretical, per [14]). We report detailed theoretical calculations in Table 2.6.

electrochemical couple	**Ni/Zn**	**Ag/Zn**
theoretical voltage	1.73V	1.5V
specific energy	100-120mAh/g	500mAh/g
commercial cell specific energy	37.5mAh/g	29-76mAh/g
commercial cell energy density	106mAh/cm^3	48-142mAh/cm^3
commercial cell capacity	0.03mAh	20-180mAh
commercial cell additives	unknown	unknown
theoretical capacity of a 0.25 mm^3 cell	0.17mAh	0.94mAh
effective capacity of a 0.25 mm^3 cell	0.026mAh (commercial cell)	0.012-0.035mAh (commercial cell)
theoretical lifetime at 12 nA discharge current	1.6 years	9.0 years
effective lifetime at 12 nA discharge current	0.25 years (~ 3 months)	0.34 years (~ 4 months)

Table 2.6. Theoretical calculations for Ni/Zn and Ag/Zn electrochemical couples [14,16,28,29,30].

In Fig. 2.5 we report the discharge profile for battery IOS-1. The output voltage measured after the battery was fabricated and connected to the discharge setup (Fig. 2.2) was ~1.5V. The cutoff voltage for the discharge test was set to 0.8V. The initial current draw was 136.0nA. From the discharge profile (Fig. 2.5) we estimate the cell capacity. For this estimate, we select a cutoff voltage of 1.11V, corresponding to a time of 6.7 hours of operation. Thus the experimental capacity for battery IOS-1 was 0.67μAh.

Based on the 4.9mm^3 cell volume we extrapolate a theoretical capacity of 1.7mAh, for an energy density of 525Wh/L [14].

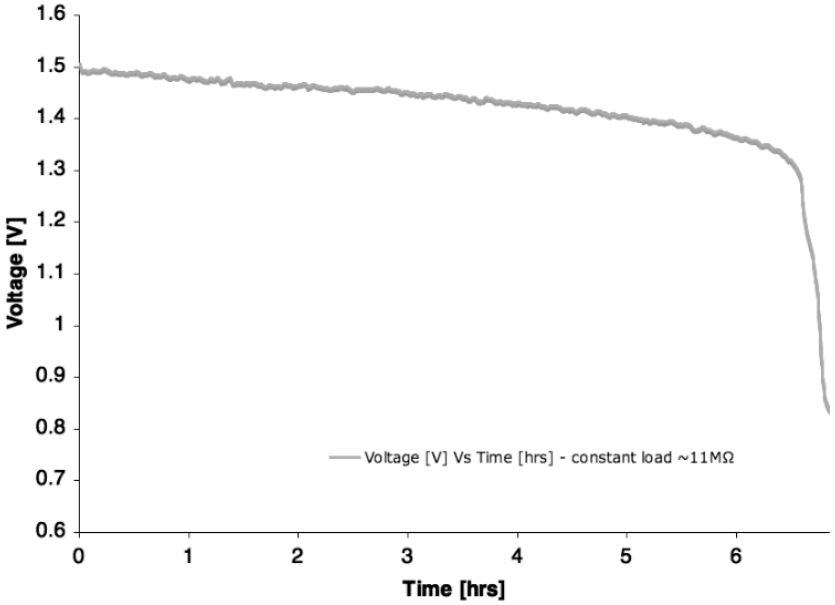

Figure 2.5. Discharge profile for battery IOS-1.

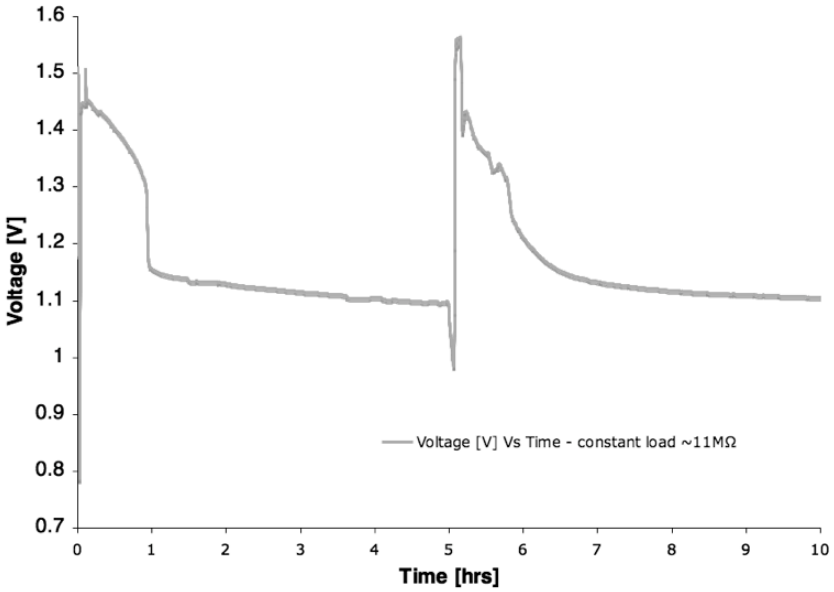

Figure 2.6. Discharge of IOS-2, showing the effect of electrolyte insertion during discharge.

In Fig. 2.6 we report the discharge profile for battery IOS-2. The output voltage measured after the battery was fabricated and connected to the discharge setup (Fig. 2.2) was ~1.5V. The cutoff voltage for the discharge test was set at ~1.1V. The initial current draw measured was 136nA. The voltage profile shows the effect of the electrolyte depletion from the reaction chamber due to lack of hermetic seal. After new electrolyte was inserted, a new peak of ~1.6V was recorded.

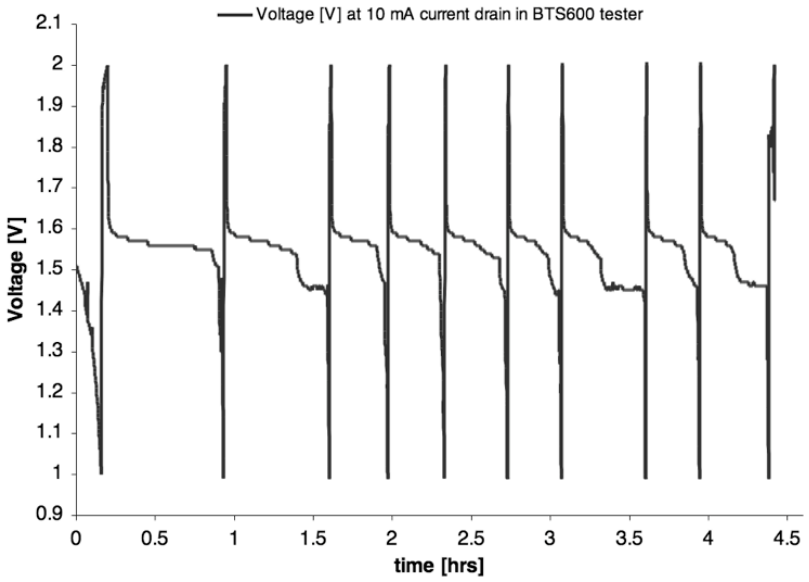

Figure 2.7. Dicharge and recharge profiles for 10 cycles, IOS-2.

After battery IOS-2 reached a voltage of 1.1V for the second time, we investigated rechargeability; results are reported in Fig. 2.7. The battery was cycled 10 times at a current draw of 10mA, which corresponds to a rate of C/5. The 10 cycles were run over approximately 4.5 hours. From the first discharge cycle (Fig. 2.7), we estimate the experimental capacity of cell IOS-2 to be ~7.7mAh, and we evaluate the theoretical

capacity based on the mass of the active materials as follows. The anode material (Zn) has a specific capacity of 0.82Ah/g [14], thus 0.026g utilized theoretically produced 21mAh. The cathode material (AgO) has a specific capacity of 0.43Ah/g [14], thus the 0.069g introduced theoretically produced 30mAh. Therefore, the overall cell theoretical capacity was calculated to be 21mAh.

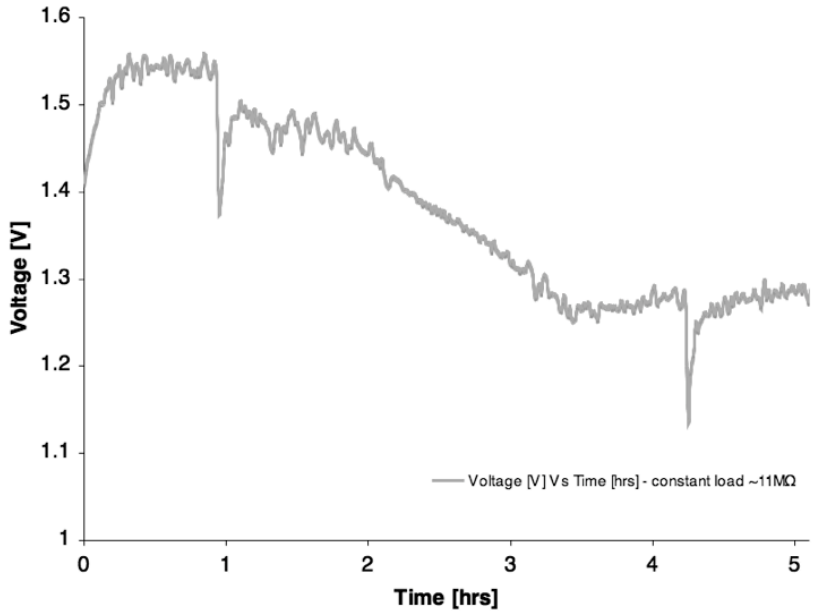

Figure 2.8. Discharge profile for IOS-3.

In Fig. 2.8 we report the discharge profile for battery IOS-3. As before, the initial voltage was ~1.5V; the test was terminated at a voltage ~1.2V. From the discharge profile (Fig. 2.8), we estimate an experimental capacity of 0.69µAh, while we used the masses of active materials to evaluate the theoretical capacities. Battery IOS-3 was built using a package of ~0.56mm^3, i.e. approximately 1/10 that of battery IOS-1. The amount of anode (Zn) material utilized for this battery was 0.0060g, providing a theoretical capacity of 4.9mAh. The amount of cathode (AgO) material employed for this cell was 0.0040g,

providing 1.7mAh. Overall, the calculated theoretical capacity for battery IOS-3 was 1.7mAh. We attempted to recharge the battery using a 1.5V alkaline commercial cell, but the original voltage was not reached and the cell self-discharged.

battery #	volume [mm^3]	theoretical capacity	experimental capacity	projected lifetime (as a primary cell) @ 12nA draw
IOS-1	~4.9	1.7mAh	0.67μAh	56 hours
IOS-2	~60	21mAh	7.7mAh	73 years
IOS-3	~0.56	1.7mAh	0.69μAh	57 hours

Table 2.7. Characteristics and performance: IOS-1, IOS-2 and IOS-3.

In Table 2.7 we summarize the projected lifetime for the batteries produced in this study, as calculated by dividing the cell experimental capacity by the specified discharge current (12nA). Microbatteries IOS-1 and IOS-3 achieved the projected lifetime of more than 50 hours, while microbattery IOS-2 shows a projected lifetime one order of magnitude above the required two years; cell volumes (mm^3) and capacities (Ah) are also presented in Table 7.

DISCUSSION

Promising steps towards the reduction in sizes of power supplies have been made, through application of lithographic techniques [20], thin-film technology [21] and rechargeable and caseless designs [22,23]. Yet, the size reductions achievable through

use of secondary versus primary systems, or thin film versus thicker electrodes, are actually less than those attainable simply by employing a hybrid architecture. Indeed, combining these strategies appears to be the most promising route.

Such hybrid systems have been developed for a variety of applications, often with excellent results in reduction of total system size and mass. A hybrid battery system comprised of two cells, a 6.0V $LiMnO_2$ and a 3.0V Li-iodine cell was proposed to replace the existing power supply of a defribillator cardioverter [13]. The new system presented a ~15% reduction in volume and ~5% reduction in mass, compared to the original unique battery (a bigger 6.0V $LiMnO_2$ cell), while the capacity increased by ~40%. A hybrid system composed by a battery and a solar cell was proposed [24] to power a generic multielement microsystem for portable wireless applications [25]. The concept system resulted in a theoretical size reduction of ~98% compared to using just one custom-fabricated battery. The solution to the challenges posed by the power demands of MEMS devices such as the WIMS-ERC EMT [10] or the WIMS-ERC Amadeus cochlear implant [11] were only possible by applying a hybrid approach, combining primary and secondary systems, high energy and power dense systems.

Though the prototype batteries produced in the present study do not yet meet the small scale required for the WIMS-ERC IOS of 1600x800x200μm^3, they did provide proof-of-concept on capacity and lifetime. In order to achieve the small size required, reduction in packaging will be required. Caseless battery systems have been proposed [22,23] for implantable MEMS applications. The Mg/AgCl and Mg/CuCl batteries [22] comprised minimum volumes of ~144mm^3 and had capacity of 1.8mWh; if scaled down to the 0.256mm^3 required by the present application, the theoretical lifetime at 12nA

would be ~ 30 days. Even if the lifetime could be increased, our main concern with implanting this system without a casing is inherent risk in the pressure build up that hydrogen bubbles in Mg/AgCl systems can produce [22]. The Zn/AgCl system proposed by the second group comprised a volume of ~ 0.1mm^3, which would be suitable for the present geometry, yet the lifetime at 12.0nA would be only ~4 hours, making it unsuitable for the present application. The glucose/O_2 systems proposed, capable of providing a tenfold increase in energy density, and consequently lifetime (5000 Wh/L vs 500 Wh/L of Zn/AgCl system [23]), are based on a cathode material (bilirubin oxidase) that is not stable [23]. It seems very unlikely, given potential toxicity, that stabilizing additives (mainly heavy metals) could be used in these systems without a package.

The IOS-1 cell capacity (0.67μAh, estimated at 1.11V cutoff voltage after 6.71 hours of discharge under a current draw of 136.0nA) was significantly less than the theoretical capacity of 1.7mAh (based on an energy density of 525Wh/L [14]). This four order-of-magnitude difference was likely the result of several well-known factors. One of these is likely incomplete filling with electrolyte. Another factor is related to electrode design; the reduced size of the electrodes (~4.9mm^2) and their flat geometry only allow limited active material surface area to be accessible to the electrolyte.

Batteries IOS-1 and IOS-3 achieved 0.01% of theoretical capacity, while battery IOS-2 achieved 15%, as calculated by multiplying the discharge current by the discharge time required to reach the cutoff voltage (reported in Table 2.7). This latter result compares favorably with other microbatteries in the literature. For example, Ni/Zn microbatteries and Li thin film batteries, which have achieved which have achieved ~7% [16] and ~12% [21] of theoretical capacity, respectively. Losses occur because of

capacity fade related to the discharge rate, low surface area of active material, and lack or depletion of the electrolyte. Clearly, work is needed on identifying the optimum discharge rate, on improving the morphology of the active material and on achieving and preserving 100% full electrolyte within the reaction chamber.

Electrolyte management remains a challenge for other, operational reasons in addition to its role in loss of capacity. Not only is electrolyte insertion difficult because of the reduced size of the package, but it is practical only before the package is sealed, and complicated by capillary forces. In Fig. 2.6 we show how the addition of new electrolyte restores the initial value of the voltage for cell IOS-2. This result shows how a complete fill of the reaction chamber with electrolyte is fundamental to obtain a capacity value closer to nominal. Moreover the inlet and outlet channels in cell IOS-2 allowed better control of the amount of electrolyte inserted into the cell casing. The voltage drop in Fig. 6 is entirely due to the electrolyte depletion, and not to actual discharge, since the starting voltage was completely restored by the operation of replenishing electrolyte into the chamber.

The cell lifetime (>50 hours for IOS-1 and IOS-3), estimated in Table 2.7 (by dividing the cell experimental capacity by the specified discharge current, 12.0nA) was significantly less than the theoretical one (60-80 years). Similarly, for IOS-2, the actual lifetime was only 10% of the theoretical. This compares favorably with other microbatteries in the literature (Zn miniature batteries [23] projected a lifetime of 2-4 weeks, i.e. 2% of similar commercial systems lifetimes (1-3 years); Ni/Zn and Li-ion microbatteries [26] achieved ~25% increase in lifetime due to electrolyte management and sealing). Microbattery IOS-3 showed a capacity, and consequently a lifetime,

comparable to IOS-1, even with a size approximately ~10 times smaller, because of the efficient electrolyte filling and package seal. Lower lifetimes resulted from capacity fade, related to the discharge schedule and depletion of the electrolyte.

Clearly, work is needed on identifying the optimum discharge schedule of our system and on improving the electrolyte management and package seal. Battery IOS-2 achieved a projected lifetime (without recharge) ~30 times higher than required. This is mainly due to the larger size and capacity of this cell, but is also related to the fabrication technique. A complete electrolyte fill of the reaction chamber enabled a higher output capacity. The cycling test for IOS-2 was run for approximately 4.5 hours, and produced 10 cycles of discharge/recharge. For determining the actual cycle life of this battery, which was not an objective of the present paper, extensive cycling tests will be required.

CONCLUSIONS/FUTURE WORK

Our study demonstrated the feasibility of design and construction of a microbattery, by optimizing both geometry and electrochemistry through careful analysis of a load profile. We developed Zn/AgO fabrication technique, demonstrated for three prototype cells: IOS-1, IOS-2 and IOS-3. Cells volumes were ~4.9mm^3, ~60mm^3 and 0.56mm^3, respectively, with experimental capacities of 0.67μAh, 7.7mAh and 0.69μAh (see Table 7). The original commercial system (Renata 317) had a volume of 43.6mm^3 of and a nominal capacity of 10.5mAh.

Cells IOS-1 and IOS-3 were discharged at 136nA; cell IOS-2 was discharged at both 136nA and 10mA. Ten complete discharge and recharge cycles were successfully obtained for cell IOS-2. Package size reduction is a key objective to achieve in order to

integrate the battery with the IOS and make it an IPS. In order for this battery to be implanted, a perfect seal of the package is required. In the present work, we studied the effects of package seal and electrolyte depletion on cell rechargeability and lifetime, but we have not yet investigated the durability of the seal for long-term implantation.

Compared to other microfabricated power systems, these Zn/AgO cells present a higher energy density and a flatter discharge curve, which makes them suitable for MEMS applications. By refining the fabrication techniques and cell design developed in this study, it should be possible to build batteries that have a longer lifetime. At present, the microbatteries do not yet meet the rigorous volume requirements ($0.256mm^3$) of the IOS; the smallest of our prototypes (IOS-3) is approximately 50% bigger than the required size. Mass constraints have also been neglected in the current work. The present package of IOS-3 (~0.1g) comprises almost 80% of the battery total mass.

The capability to recharge this electrochemistry can extend the ultimate lifetime of the device and allow a longer permanent implantation. Future work will entail continued evaluation of the hermetic package seal, while also consideration of reduction of mass. At present, a set of microbatteries is being constructed for a fully integrated testbed, to assess their nominal capacity and effective lifetime.

BIBLIOGRAPHY

1. Wise, K. D., Silicon microsystems for neuroscience and neural prostheses. IEEE Engineering in Medicine and Biology Magazine, 2005. 24 (5): p. 22-29.

2. Simunic, T., Benini, L., De Micheli, G., Energy-efficient design of battery-powered embedded systems. IEEE Transactions On Very Large Scale Integration (VLSI) Systems, 2001. 9: p. 15-28.

3. Greatbatch, W., Implantable power-sources: a review. Journal of Medical Engineering and Technology, 1984. 8: p. 56-63.

4. Greatbatch, W., Twenty-five years of pacemaking. Pace, 1984. 7(January-February): p. 143-147.

5. Jeutter, D.C., A trans-cutaneous implanted battery recharging and biotelemeter power switching-system. IEEE Transactions on Biomedical Engineering, 1982. 29(5): p. 314-321.

6. Ikeda, H., Furukawa N., Narukawa, S., Yoshizawa, S., Energy source for the middle ear implant. Advances in Audiology, 1988. 4: p. 73-84.

7. Mussivand, T., Hum, A., Diguer, M., Holmes, K.S., Vecchio, G., Masters, R.G., Hendry, P.J., Keon, W.J., Canada -- transcutaneous energy and information transfer system, in ASAIO Journal (41/3 (M253-M258) 1995). Biosensors and Bioelectronics, 1996. 11: p.IV.

8. Baumann, J.W., Leysieffer, H., Basics of energy supply to completely implantable hearing aids for sensorineural hearing loss. Hno, 1998. 46(2): p. 121-128.

9. Shapiro, S., Borgens, R., Pascuzzi, R., Roos, K., Groff, M., Purvines, S., Rodgers, R.B., Hagy, S., Nelson, P., Oscillating field stimulation for complete spinal cord injury in humans: a Phase 1 trial. Journal Neurosurgery-Spine, 2005. 2: p. 3-10.

10. Cook, K. A., Sastry, A. M., An algorithm for selection and design of hybrid power supplies for MEMS with a case study of a micro-gas chromatograph system. Journal of Power Sources, 2005. 140 (1): p. 181-202.

11. Cook K. A., Albano, F., Nevius, P., Sastry, A. M., POWER (power optimization for wireless energy requirements): a matLab based algorithm for design of hybrid energy systems. Journal of Power Sources, 2005. 159 (1): p. 758-780.

12. Wu, Q., Qiu, Q., Pedram, M., An interleaved dual-battery power supply for battery-operated electronics. IEEE (Ed.), Asia and South Pacific Design Automation Conference, Yokohama, Japan, 2000. p. 387-390.

13. Drews, J., Wolf, R., Fehrmann, G., Staub, R., Development of a hybrid battery system for an implantable biomedical device, especially a defibrillator cardioverter (ICD). Journal of Power Sources, 1999. 80: p. 107-111.

14. Linden,D., Reddy,T.B., Handbook of Batteries-3rd Edition, McGraw-Hill, New York, 2002. p. 12.1.

15. http://www.bipolartechnologies.com/Microbattery2.htm, accessed February 7th 2007.

16. Singh, P., Wang, X.Q., LaFollette, R., Reisner, D., RF charged microbattery for powering miniature sensors, Proceedings of the IEEE Sensors, 2004. 1-3: p. 349-352.

17. http://www.corning.com/docs/specialtymaterials/pisheets/Macor.pdf, accessed January 28th 2007.

18. http://www2.dupont.com/Separation_Solutions/en_US/tech_info/spunbonded/spunbound_poly.html, accessed February 16th 2007.

19. http://www.emersoncuming.com/other/2850ft.pdf, accessed February 7th 2007.

20. Humble, P.H., Harb, J.N., LaFollette, R.M., Microscopic nickel–zinc batteries for use in autonomous Microsystems. Journal of The Electrochemical Society, 2001. 148: p. A1357-A1361.

21. Neudecker, B.J., Dudney, N.J., Bates, J.B, 'Lithium-free' thin-film battery with in situ plated Li anode. Journal of The Electrochemical Society, 2000. 147: p. 517.

22. F., Sammoura , , K.B., Lee and L. Lin, "Water-activated disposable and long shelf life microbatteries," Sensors and Actuators A: Physical, 2004. 111 (1): p. 79-86.

23. Heller, A., Potentially implantable miniature batteries. Analitical and Bioanalitical Chemistry, 2006. 385: p. 469–473.

24. Harb, J.N., LaFollette, R.M., Selfridge, R.H., Howelld, L.L., Microbatteries for self-sustained hybrid micropower supplies, Journal of Power Sources , 2002. 104 (1): p. 46-51.

25. Mason, A., Yazdi, N., Chavan, A.V., Najafi, K., Wise, K.D., A generic multielement microsystem for portable wireless applications. Proceedings Of The IEEE, 1998. 86: p. 1733-1746.

26. LaFollette, R.M., Harb, J.N., Humble, P., Microfabricated secondary batteries for remote, autonomous, electronic devices. Sixteenth Annual Battery Conference On Applications And Advances, 2001. p. 349-354.

27. Conceptual device, WIMS-ERC intraocular Testbed, (July, 2005).

28. http://www.powergenixsystems.com, accessed October 7th 2005.

29. http://www.yardney.com, accessed October 7th 2005.

30. http://www.duracell.com/procell/chemistries/silver.asp, accessed October 3rd, 2005.

CHAPTER III

A FULLY INTEGRATED MICRO- BATTERY FOR AN IMPLANTABLE MICROELECTROMECHANICAL SYSTEM[1]

INTRODUCTION

The reduction in size and improvement in capability of microsystems (e.g. those in Figure 3.1a and 3.1b) is presently limited by the specific and gravimetric properties, and overall sizes, of on-board power supplies [1]. This is most readily seen in autonomous devices used in environmental [2] biological [1,3] and medical [4,5,6] applications (Table 3.1), which rely mainly on batteries for power. Indeed, power supplies often comprise up to ten times the mass of the other elements of the system.

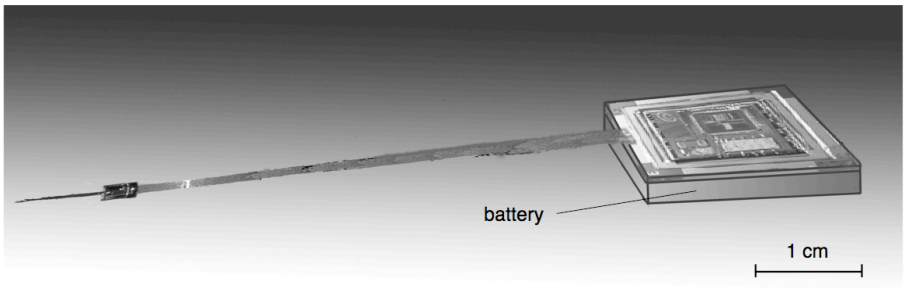

Figure 3.1a. WIMS-ERC Amadeus CI with integrated battery [41].

[1] Material in this chapter is a unpublished paper in progress: F. Albano, Y.S. Lin, S. Hanson, D. Blaauw, D. M. Sylvester, K. D. Wise and A.M. Sastry, "A Fully Integrated Micro- Battery for an Implantable Microelectromechanical System," Journal of Electrochemical Society, 2008.

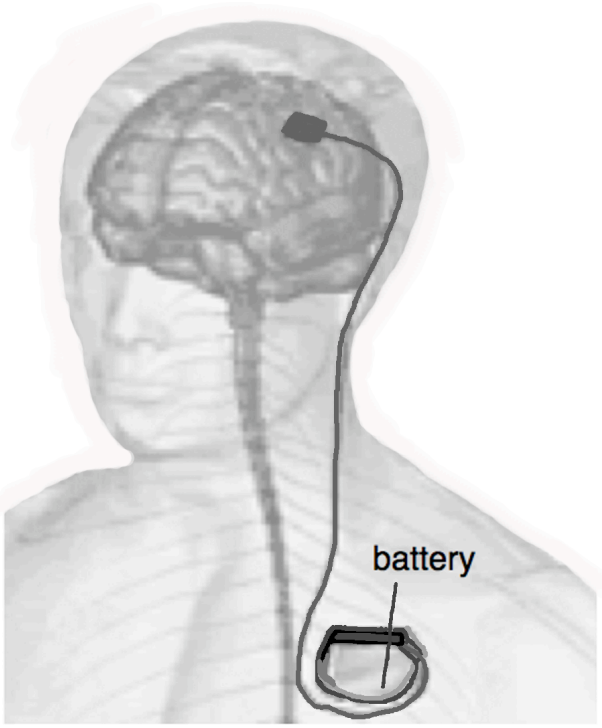

Figure 3.1b. Northstar Neuroscience, neurostimulator adapted from [42].

Typical batteries used for these devices are Zn-air, Li metal, Li-ion or Zn/AgO, with costs ranging from 0.5 to 2.5$/Wh [7]. Despite their excellent energy per unit volume (Table 3.2), thin film batteries (TFBs) require surface areas O~cm^2 in order to power MEMS devices for times greater than one day, preventing their application. Because of the inability to obtain scale-appropriate TFBs to date, successfully demonstrated devices have been powered with macroscopic power sources (Table 3.1) while TFBs have only been investigated for potential applications but never implemented or integrated in a complete device. The WIMS-ERC intraocular sensor, selected for our study, illustrates a critical issue concerning all microscopic power designs and their integration on-board autonomous MEMS devices. Possibly the most significant development in autonomous MEMS in the coming decades, for new applications, will be the achievement of fully

integrated and optimized power supplies, realized cost-effectively, that are also capable to achieve energy densities (~27mWh/cm^2 [8]) required to operate MEMS.

Considerable work has been performed to achieve such power elements (Table 3.2), independent of specific applications, including the present work. Li-ion microbatteries [9,10,11,12,13,14] have been widely investigated because of their high nominal voltage (~3.7V), giving them a much higher capacity than other electrochemistries, e.g. Ni/Zn (~1.8V) [15,16,17] or Ag/Zn (~1.55V). Very low thicknesses, ranging from ~15μm (Li-ion) to ~100μm (Li-ion, Ni/Zn, Ag/Zn) have been achieved; however microelectronics and MEMS applications, requiring high capacity (up to 20mAh/cm^2 [8]), cannot presently be powered by such intrinsically low capacity technologies. Though power densities as high as 30-70mW/cm^2 have been achieved by microbatteries, their low capacity (maximum ~100μAh/cm^2 achieved in commercial TFBs [18]) remains a major limitation. More recently, 3D electrode architectures have demonstrated increased specific capacities (e.g. 3.5mAh/cm^2 [19], and 500mAh/g [20]) allowing use of batteries with greatly reduced surface areas.

Table 3.1. Survey of battery powered MEMS [1-6].

microsystem	application	system volume (no battery)	battery volume	system mass (no battery)	battery mass	battery chemistry	clinical test	year	ref.
cyborg beetle	micro air vehicle (MAV)	$3mm^3$ (no electrodes)	$110mm^3$	262mg	400mg	Zn-air	Green June Beetle (*Cotinis Texana*)	2008	[1]
multi-sensor	environmental/ biological monitoring	$0.15cm^3$	$0.35cm^3$	0.25g	3g	lithium	n/r	2006	[2]
bio-potential recording system	biological potential monitoring	$7.3x10^{-3}mm^3$	$326mm^3$	1.1g (with battery)	n/r	n/r (1.5V)	marmoset monkey (*Callithrix Jacchus)*	2005	[3]
microelectronic pill	remote biomedical measurements	$0.5mm^3$	$1,183mm^3$	7.0g	5.2g	Zn/AgO	n/r	2004	[4]
nerural recording system	neural recording	$351cm^3$	$161cm^3$	195g	40g	Li-ion	rhesus macaque (*Macaca mulatta*) owl monkey (*Aotus nancymae*)	2004	[5]
radio-transmitter	neural recording	$1.25cm^3$	$0.8cm^3$	3.1g	1g	Zn-air	behaving barn owls (*Tyto alba*)	2000	[6]

Table 3.2a: Survey of microbatteries [5,9,10,12,13,14,15,16,17,18,24,45,46,47,48].

year	1995	2006	2002	2000	2000	1995	2007	2007	2001	2007
process	sputtering, thermal evaporation	RF-sputtering	sol-gel, spin coating	sputtering, thermal evaporation	sputtering, thermal evaporation	sputtering, thermal evaporation	vacuum evaporation	LPCVD, sputtering etching	sputtering, electroplating	PVD
cathode	V_2O_5	V_2O_5	$LiMn_2O_4$	$LiCoO_2$	Mn_2O_4	TiS_2	$LiCoO_2$	Pt	NiOOH	AgO
anode	Li	Li	Li	Li	Li	Li	Li	Al	Zn	Zn
electrolyte	LIPON	$LiClO_4$(aq)	SiO_2/P_2O_5 glass	LIPON	solid Li glass	solid Li glass	LIPON	KOH/K Cl/H_2O_2	20%wt KOH-ZnO	27%wt KOH
nominal voltage [V]	3.75	3.8	4.2	4.0	4.0-4.5	2.5	3.9-4.2	0.8-1.3	1.7-1.8	1.55
thickness [μm]	7-15	3.6	6-8	2.2*-15	0.3*	8-12	110	6	100	25
area [cm^2]	1.21	0.5	2E-4	1.0*-3.22	1.0*	1.0	6.45	1.0	0.007*-0.02	1.0
capacity [μAh]	13.5-18.5	50	1.96E-3	160	15	n/r	700	64	1.9-6.79	100
discharge current [μA]	2.42-48.4	50	28nA	100	10	n/r	n/r	240	n/r	250
C-rate	C/8-5C	8C	14C	1.6C	1.5C	n/r	n/r	3.75C	n/r	2.5C
$\tilde{c}$ [μAh / cm^2]	20-120	100	9.6	60-150	20-60	35-100	108	400	277-970	100
$\hat{i}$ [μA / cm^2]	2-40	0.1mA/cm^2	140	100μA-4mA/cm^2	n/r	n/r	n/r	240	7-100mA/cm^2	250
$\hat{p}$ [mW / cm^2]	n/r	n/r	0.6	30	30	n/r	n/r	4.8-6.5	70	0.4
$\hat{e}$ [Wh / L]	425	n/r	68.6	2070	n/r	n/r	40	300-600	55	40
reference	[1]	[2]	[3]	[4-8]	[4-8]	[6,12,14]	[9]	[10]	[11-13]	[15]

* = cathode only $\tilde{c}$ = specific capacity $\hat{i}$ = current density $\hat{p}$ = power density $\hat{e}$ = energy density

Systems requiring complicated power profiles (e.g. high pulses, spikes or steady plateaus) or comprising subcomponent devices (e.g. the electrode array in the WIMS-CI [21] and the heating column in the WIMS-EMT [22]), provide an opportunity for hybridization of power supplies [23], comprising of more than one cell and/or electrochemistry. Two Li-ion batteries targeted different components of the WIMS-CI and hypothetically enabled a fully implantable device by extending its lifetime up to 48 years (by assuming a continuous usage of the device for 16 hours a day and recharge at 20% depth of discharge; capacity fade was also accounted for in the calculation); a thin-film battery coupled with a Li-ion cell comprised the power source designed for the WIMS-EMT reducing its mass and volume by three orders of magnitude compared to using only one battery.

At present there are essentially no thin film batteries that have footprints smaller than $1cm^2$, can achieve capacities higher than 100μAh or that have lifetimes longer than one day, while still comprising reasonable cost (~$300/Wh [18]). Size reduction and increase in electrode capacity (3D electrodes) have scaled with manufacturing costs, due to the extensive usage of clean room facilities and low volume of manufactured products. Outside-the-clean room manufacturing may reduce cost. In-situ manufactured batteries, directly on the chip case or the chip carrier are only possible if the fabrication conditions are benign for MEMS production. Thus, both temperature (<800ºC [11]) and use of etchants and solvents [16,20] are limited. Lastly the high voltage of Li chemistries, widely proposed as thin film batteries material, makes them less suitable for intrinsically low power MEMS devices [27,28] or where operational amplifiers cannot be used to reduce the battery output voltage.

Adopting manufacturing techniques that can be performed outside-the-clean room [24], which are also compatible with CMOS fabrication techniques, have the potential to enable batteries to be built at the same time as the microsystem, having the same scale of other components, optimizing its mass and volume and saving several processing steps.

Thus, in the present study, we set four objectives:

1) select and designing an optimized power supply for the WIMS-IOS [23];

2) develop a fabrication technique that allows small scale, low-cost, and integrable fabrication for CMOS systems, and experimentally demonstrate a microscopic power source entirely fabricated using such a procedure;

3) map capacity and lifetime of several fabricated microbatteries; and

4) determine the effects of miniaturization on the power source performance and on the device architecture.

Our methodology builds on our prior efforts in the area, including optimization of power supplies [21,22], manufacture of novel microbatteries [23,24] and electrode optimization [25,26].

METHODS

TESTBED

The WIMS-ERC intra-ocular sensor (IOS), an implantable microsystem of less than ~0.4mm^3 volume and ~2mm^2 footprint, implanted inside the eye for 6 months to 2 years to monitor glaucoma patients intraocular pressure (Figure 3.2a and 3.2b), was used as testbed for our microbatteries.

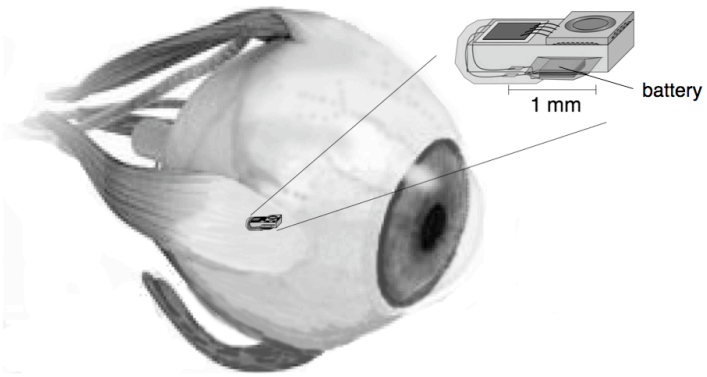

Figure 3.2a: WIMS-ERC IOS implant location

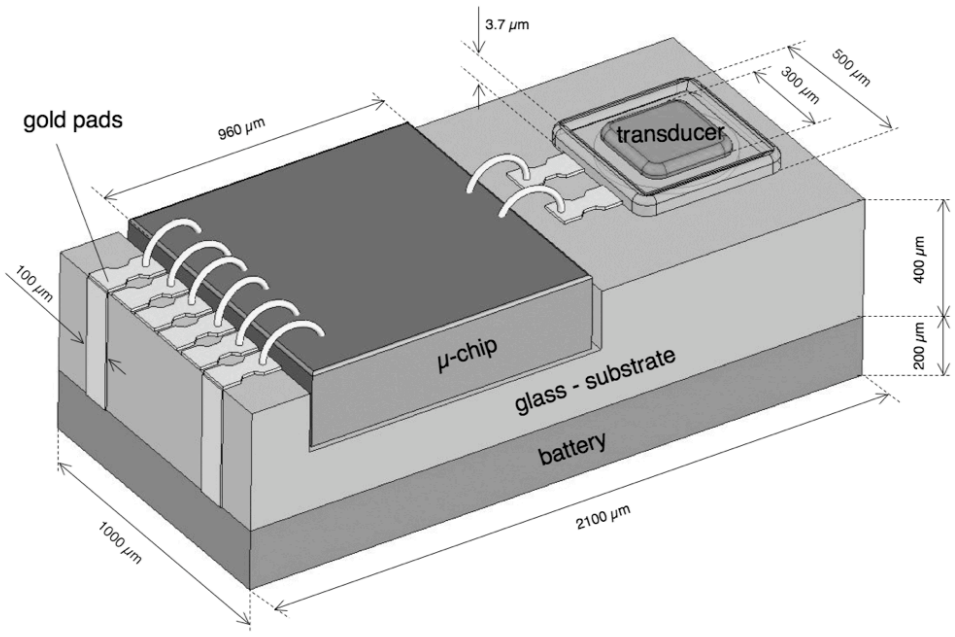

Figure 3.2b: WIMS-ERC IOS with integrated battery [43].

This device is based on the Phoenix Processor [27,28], an ultra low power consumption platform (~30pW) used in several WIMS microsystems. Its bimodal duty cycle (Figure 3.3) comprises ~10 minute periods of "sleep," punctuated by 30-50ms (milliseconds) "active" sensing periods (Table 3.3a). Extrapolation of a monthlong

profile was accomplished by considering a constant voltage step of 1.5V at a constant current draw of 100nA during 1hr, repeated 720 times to cover a 1-month period (Table 3.3b). Voltage regulation in the chip is necessitated by operation and control, at different voltages, of several components, and it is accomplished (Figure 3.6) by use of a DC/DC converter capable of converting variable voltages ranging 1.0-1.6V down to constant voltages of 0.1-0.4V. The geometric constraints imposed to the design of the power supply were a surface area of 1 to 3mm^2 (i.e. the entire area above the chip surface or up to the entire area on the back of the device substrate) and a volume of ~0.42mm^3 (Figure 3.2b).

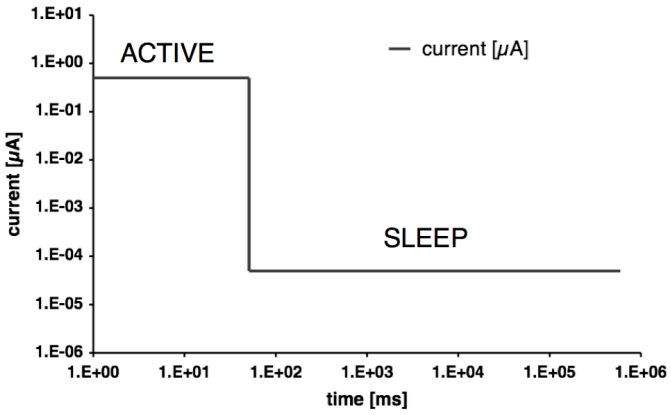

Figure 3.3: WIMS-ERC IOS microchip DC

elapsed time	voltage [V]	current draw
10 min	0.5V	50pA
30-50ms	0.5V	100-500nA (max 1μA)

Table 3.3a: WIMS-IOS: microchip power draw (single DC).

number of cycles	cycle duration	voltage	current draw	total capacity	total energy
720	3600s (1hr)	1.5V	100nA	72μAh	0.1mWh

Table 3.3b: WIMS-IOS: 1-month draw cycle.

BATTERY DESIGN AND FABRICATION

After the power profile and constraints (geometrical, environmental, lifetime) were defined, we evaluated implementation of available commercial systems, using a previously built algorithm, POWER [21,22]. This algorithm evaluates three different optimization approaches (results in Table 3.5 are grouped by Approach 1, 2 and 3) to screen a user-defined commercial database of cells and to propose possible candidates. In our selection approaches, we included considerations of energy and power densities, coupled with models for losses in capacity over time and over cycling (secondary cells) of the cells. The current version of the database included primary silver oxide (Zn/AgO), alkaline, zinc and lithium batteries (totaling 194 cells) and secondary Li-ion, Nickel (NiMH and Ni-Zn) and lithium polymer batteries (totaling 61 cells), covering all commercially available chemistries and few research systems. As the device architecture was mostly flat, we particularly targeted electrochemistries that have planar form factors, e.g. thin film batteries (Table 3.4).

POWER version	added/removed files (compared to prev. version)	program location	# of batteries in database (p=primary, s=secondary)	operating system/ Matlab® version (used to run)	Date
1.4.3	in **battery_secondary.m** added: **1** Bipolar technologies cell NiOOH/Zn [1], **1** $LiCoO_2$ Neudecker thin film cell [2], **1** Infinitepower Li-fiber ($LiCoO_2$) [3]	sastrylab11.engin.umich.edu	p = 194 s = 61	Mac OS 10.4.9 and Windows XP/ Matlab 7.2.0.283 (2006a)	06/05/07

Table 3.4: POWER: version information, current database constitution [12,15,18].

In order to reduce the size and enable a flat form factor for the fabricated batteries (suitable for integration with MEMS), we utilized thin film electrodes construction. Sub-μm metallic layers of Au, Ag, Ni and Zn were deposited onto glass (SiO_2) and metallic (Cu) substrates using physical vapor deposition (PVD) and aerosol spray of metal nanopowders [29]. To maintain fabrication costs low and facilitate scalability of the process, deposition of the films was conducted outside-the-clean room in a vacuum deposition chamber type EvoVac® A-Mod [30] (Figure 3.4) from Ångstrom Engineering. A pressure of the order of 10^{-7} Torr was maintained inside the chamber while metal particles of few millimeter diameters were melted and evaporated into gas phase. The deposition substrate was attached to a rotating disk (constant speed, to grant a uniform deposition thickness) at the top of the chamber while the electrodes were deposited using a maskless approach. Deposition rates and thickness of the deposited films were monitored through multiple mass sensors located inside the chamber and controlled through the instrument software. The anode electrodes were deposited by directly spraying zinc (Zn) nanopowder on top of the metal current collector (Cu) at room temperature and atmosphere. A summary of the anode samples produced in our study is

reported in Table 3.7a. The cathode (Ag) samples were formed by vacuum deposition of titanium (Ti, for adhesion), gold (Au, for current collector) and silver (Ag, active material) layers, hierarchically on a glass substrate (Table 3.7b). After PVD was completed, the Ag films were removed from the vacuum chamber and oxidized in ozone (O3) atmosphere, using a UVO Cleaner® 342 machine for 10 and 15 minutes.

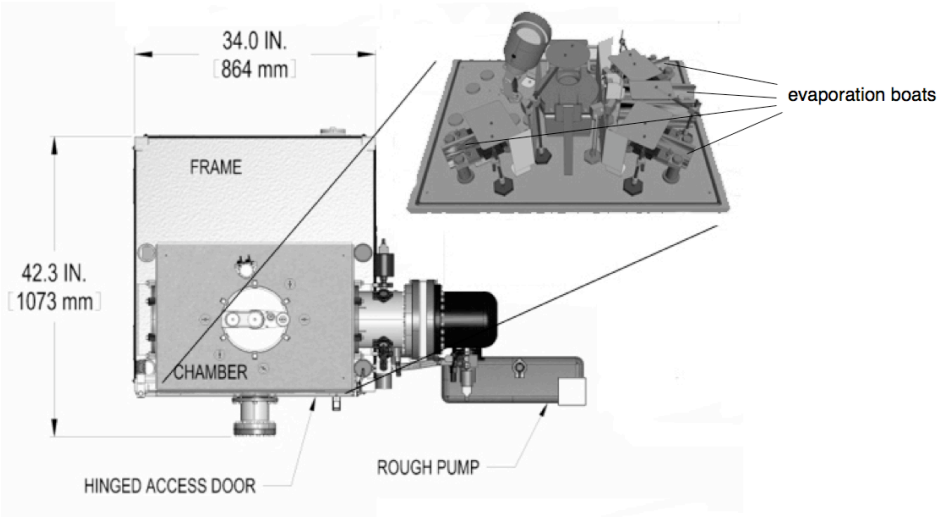

Figure 3.4: Ångstrom Engineering: EvoVac A-mod vacuum deposition system [44].

MATERIALS IMAGING

In order to quantify the morphology and microstructure of the anode and cathode films, we imaged the samples in a Philips XL30 FEG scanning electron microscope (SEM). Sizes of anode porosity and particles were recorded. Uniformity of the cathode films was qualitatively estimated by comparing the surface morphology before and after oxidation. X-ray energy dispersive spectroscopy (XEDS) capabilities of the instrument were utilized to verify the purity of the deposited samples and to detect the elemental composition of the electrodes.

DESCRIPTION OF FABRICATED PROTOTYPES

To map the influence of size over cell capacity and cycle life, we fabricated and tested six different cells, three with a larger footprint of the order of cm^2 ($O\sim cm^2$), which we will refer to as IOS-C-1, IOS-C-2 and IOS-C-3 respectively and three with a smaller footprint of the order of mm^2 ($O\sim mm^2$), which we will refer to as IOS-M-1, IOS-M-2 and IOS-X-1 respectively (summarized in Table 3.8a and 3.8b). Battery IOS-C-1 was designed to establish the capacity of thin film Zn/AgO batteries and to evaluate their cycle life at constant discharge rate. Batteries IOS-C-2 and IOS-C-3 were constructed to estimate the influence of different discharge rates and to further evaluate cycle life. Batteries IOS-M-1 and IOS-M-2 were built to evaluate the ability of reducing battery size and to study the effects of size reduction. Finally battery IOS-X-1 was fabricated to investigate the effects of system integration, variable discharge rate and size reduction at the same time.

Battery IOS-C-1 was fabricated using anode-Sample II of Table 3.7a and cathode-Sample I of Table 3.7b. A Celgard® 3401 microporous membrane (25μm thick) was used as separator. As electrolyte an aqueous solution of potassium hydroxide (28% KOH, 1% Li, from Yardney Technical Products Inc.) was employed. A hermetic seal was achieved by means of a silicone gasket and a set of Plexiglass clamps to hold all components together. The electrodes surface area was $0.7x1.7cm^2$ and the volume of the cathode was estimated to be $\sim 1.7x10^{-5}cm^3$.

All other cells utilized anode-Sample II of Table 3.7a in the construction. Cathode-Sample II of Table 3.7b was utilized to fabricate respectively two of the $\sim 1cm^2$

footprint batteries, IOS-C-2 and IOS-C-3, and two of the ~2mm^2 ones, IOS-M-1 and IOS-M-2.

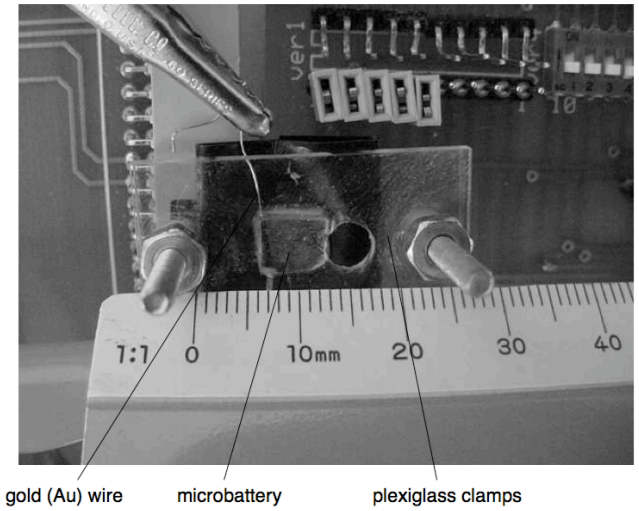

Figure 3.5: IOS-X-1: assembled microbattery.

To demonstrate integration with the powered device, battery IOS-X-1 was constructed. Cathode-Sample III of Table 3.7b was utilized following the same procedure described above. IOS-X-1 had an electrode surface area of 1.86x2.82mm^2 and an estimated cathode volume of 7.3x10^{-4}mm^3. Figure 3.5 represents battery IOS-X-1 sealed between Plexiglass clamps.

MAPPING BATTERY CAPACITY AND LIFETIME

Battery IOS-C-1 was validated, using a Solartron® 1470E battery tester, in 10 cycles of discharge and recharge at constant 250μA (~1.4C rate) current. A similar test, 10 cycles at constant 250μA (~1.4C rate) draw, was performed on battery IOS-C-3 using a Maccor® Series 4000 battery tester. Finally battery IOS-M-1 was cycled five times, in the Maccor® battery tester, at a constant 2.5μA (~0.7C rate) current.

To estimate capacity as close as possible to theoretical, battery IOS-C-2 and IOS-M-2 were discharged at a very low rate in the Maccor® tester. The first one was discharged at a constant current of 2.5μA (~C/70 rate) while the second one was discharged at a constant current of 25nA (~C/150 rate).

INTEGRATED DEVICE

The whole integrated device, microbattery IOS-X-1, DC/DC converter T68A-BE (voltage regulator) and microchip MOSIS T5AE-AA is presented in Figure 3.6. The microchip was powered initially through a power supply type Agilent E3620A maintaining a constant voltage of 0.62V. After the circuit operation was tested, the power supply was replaced by battery IOS-X-1. IOS-X-1 discharge schedule was a variable current draw imposed by the microchip. The voltage drop was recorded over time in a Keithley 6514 Pico-Voltmeter, while the current was monitored using a Keithley 6485 Pico-Ampmeter.

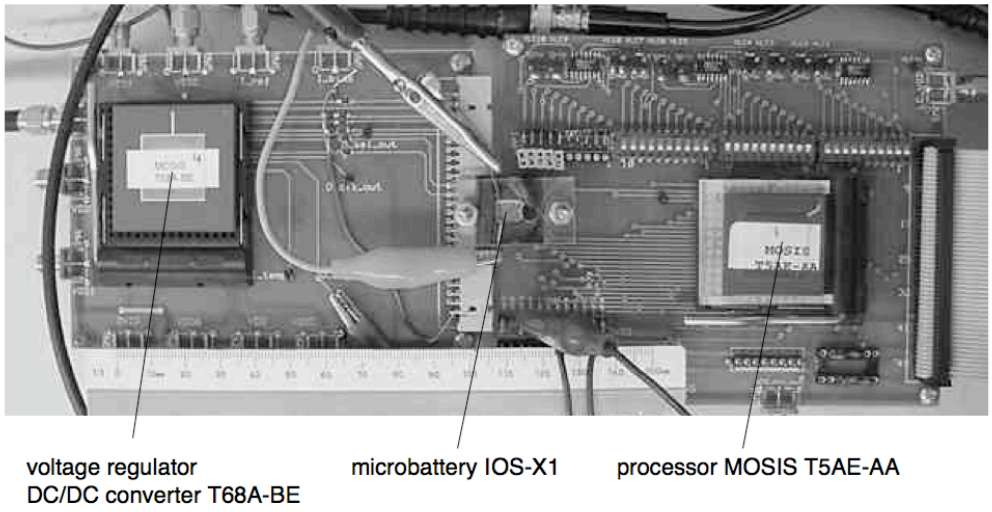

Figure 3.6: IOS-X-1: chip/battery integrated system.

RESULTS

POWER OUTPUT RESULTS

The results from POWER [21] are presented in Table 3.5. When primary cells were considered, of all 194 batteries included in the database, a Zn/AgO battery type Renata 317 was the predominant candidate. This battery had a high nominal capacity (10.5mAh), with a reduced mass (0.18g) and a volume (43.5mm^3). The resulting projected lifetimes of all three approaches exceeded the targeted lifetime (6months to 2years) by more than one order of magnitude. Among 61 secondary systems, a commercial Panasonic ML421S LiMn2O4 cell [31] and a research thin film $LiCoO_2$ cell [11] met system requirements. The ML421S cell had a capacity of 2.3mAh, with a mass of 0.11g and a volume of 38mm^3. The $LiCoO_2$ thin film battery (from the reference) had a capacity of approximately 1mAh, with a mass of 0.1g and a volume of 1.5mm^3.

primary cells:

intra-ocular chip - volume priority - 30 days of operation							
	Manufacturer	Part No.	electrochemistry	Total No.	No. of Cycles	Total Mass [kg]	Total Volume [L]
Approach 1	Renata	317	Zn-AgO	1	2.70E+02	1.80E-04	**4.36E-05**
Approach 2							
micro	Renata	317	Zn-AgO	1	2.70E+02	1.80E-04	4.36E-05
milli	n/a	n/a	n/a	n/a	n/a	n/a	n/a
watt	n/a	n/a	n/a	n/a	n/a	n/a	n/a
TOTALS				1		1.80E-04	**4.36E-05**
Approach 3							
Site 1	Renata	317	Zn-AgO	1	2.70E+02	1.80E-04	4.36E-05
TOTALS				1		1.80E-04	**4.36E-05**

secondary cells:

intra-ocular chip - volume priority - 30 days of operation							
	Manufacturer	Part No.	Electrochemistry	Total No.	No. of Cycles	Total Mass [kg]	Total Volume [L]
Approach 1	Panasonic	ML421S	$LiMnO_2$	1	63.9	1.10E-04	**4.00E-05**
Approach 2							
micro	Panasonic	ML421S	$LiMnO_2$	1	63.9	1.10E-04	4.00E-05
milli	n/a	n/a	n/a	n/a	n/a	n/a	n/a
watt	n/a	n/a	n/a	n/a	n/a	n/a	n/a
TOTALS				1		1.10E-04	**4.00E-05**
Approach 3							
Site 1	Neudecker	n/a	$LiCoO_2$	1	37.0	1.00E-04	1.50E-06
TOTALS				1		1.00E-04	**1.50E-06**

Table 3.5: POWER solution for 1-month continuous operation (volume priority).

Our secondary battery database did not include Zn/AgO secondary cells. This electrochemistry has only been used as primary systems for portable applications and as secondary systems of very large scale [32] for space and defense applications. The resulting projected lifetime of the commercial $LiMn_2O_4$ cell exceeded 5 years (63.9 cycles of a month) while the research $LiCoO_2$ battery projected lifetime was approximately half of it (37 cycles of a month). For the secondary cells lifetime estimate, rechargeability was not accounted as the required lifetime was already met when using them as primary cells.

BATTERY FABRICATION

In Table 3.6 properties and costs of metals that were deposited in our study, and of lithium compounds that were found in the previous state-of-the art TFBs, are compared.

Figure 3.7 depicts the surface of anode-Sample II of Table 3.7a. The zinc (Zn) particles were 97% pure and presented an open porous structure that was useful to capture the liquid electrolyte. Figure 3.8 shows a detail of individual Zn particles, from the same sample, having diameters of 2-8μm. The XEDS spectrum shows as the main element zinc (Zn) with some traces of carbon (C) coming from the organic solvent of the Zn spray. Figure 3.9 illustrates the cathode surface (cathode-Sample I of Table 3.7b) XEDS spectrum showing silver (Ag), oxygen (O), silicon (Si) and titanium (Ti) peaks. The XEDS spectrum only provides a qualitative measure for oxidation since the intensity of the peak does not provide the amount of detected element but only its relative abundance in the area swiped by the electron gun. Figure 3.10 depicts a larger view of cathode-Sample I with a remarkably uneven surface morphology.

metal	deposition technique	melting point T[°C]	bulk density [g/cm^3]	T [°C] @ 10^{-6} torr	Cost [$/g]
gold (Au)	PVD [1]	1962	19.32	947	33.25
nickel (Ni)	PVD [1]	1453	8.91	1072	2.4
silver (Ag)	PVD [1]	961	10.49	958	4.9
titanium (Ti)	PVD [1]	1668	4.50	1235	3.0
zinc (Zn)	PVD [1]	419	7.14	177	2.4
lithium (Li)	PVD [1]	180	0.53	307	n/r
lithium phosphate (Li_3PO_4)	thermal evaporation in N_2 atmosphere [2]	n/r	n/r	n/r	3.1
lithium cobalt oxide ($LiCoO_2$)	sputtering [2]	n/r	n/r	n/r	1.75
vanadium pentoxide (V_2O_5)	PVD [1] or sputtering [3]	690	3.36	500	0.17

1.5g metal = 500-700Å film thickness deposition

Table 3.6: PVD materials survey and physical properties [11,14,49].

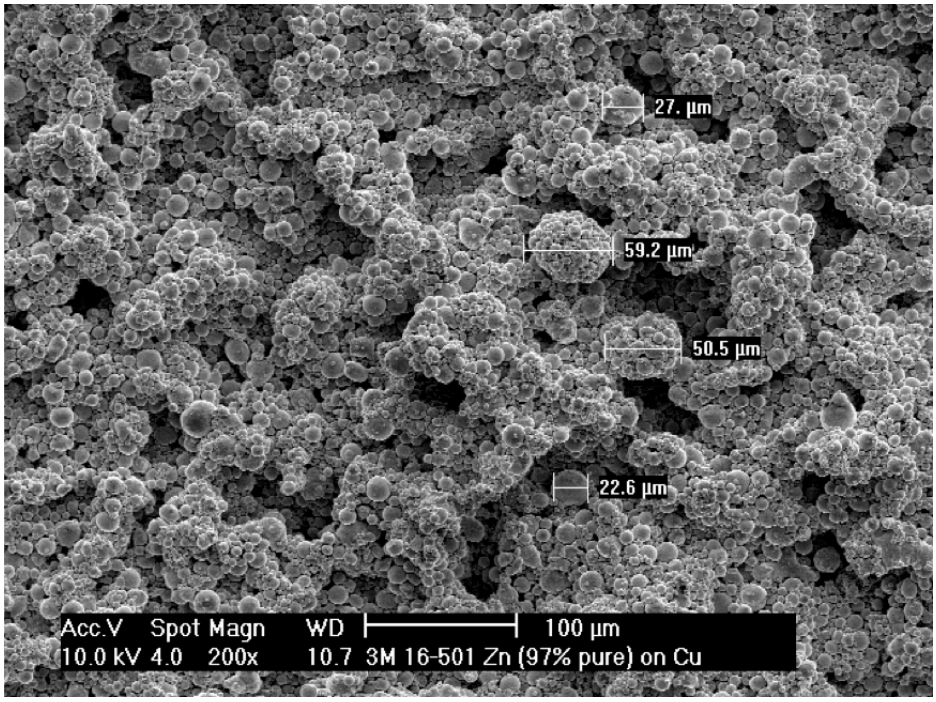

Figure 3.7: SEM picture of Zn anode surface (Sample II, aerosol spray [29] deposited).

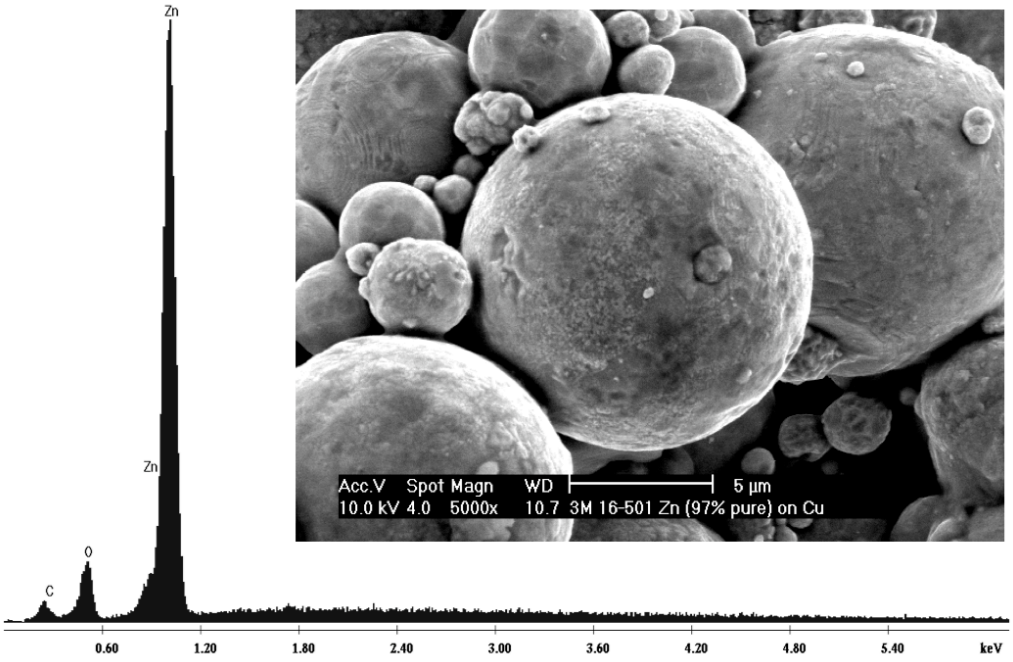

Figure 3.8: SEM picture of Zn anode (Sample II) particles and corresponding XEDS spectrum.

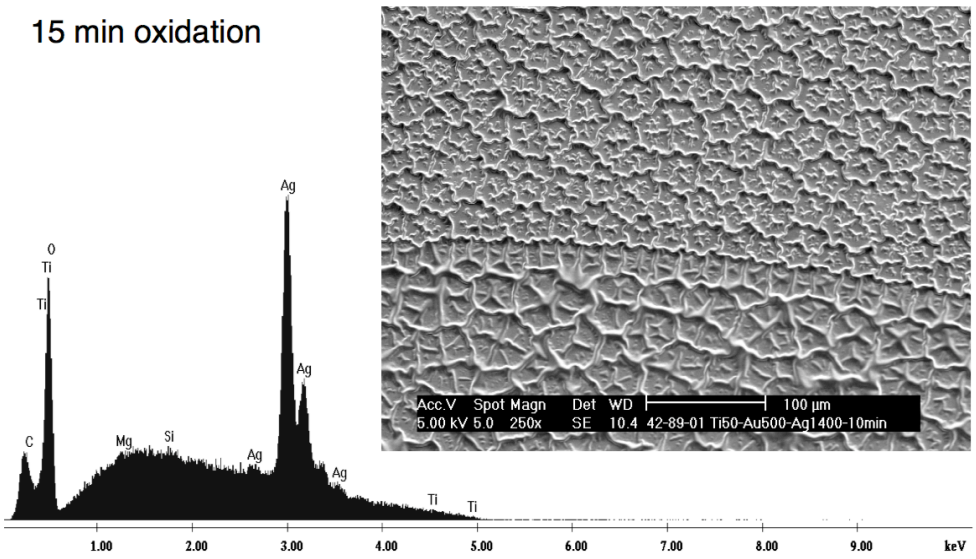

Figure 3.9: SEM picture of AgO cathode surface (Sample I, 15 min oxidation) and corresponding XEDS spectrum.

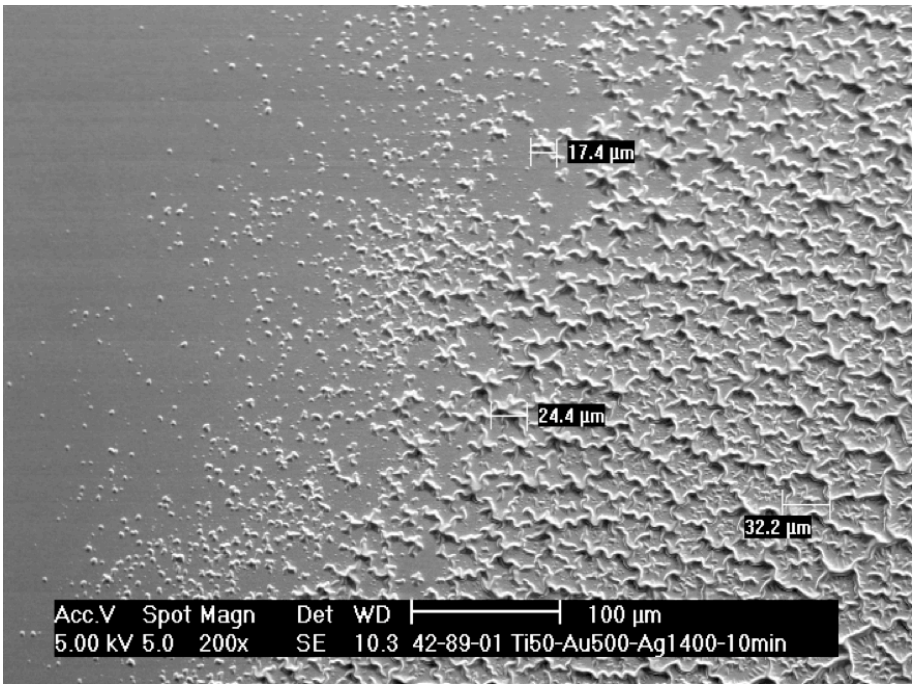

Figure 3.10: SEM picture of AgO cathode surface (Sample I, 15 min oxidation)

THEORETICAL CALCULATIONS

Very thin (~100-500nm) electrode thicknesses, suitable for MEMS power sources, with capacities up to 75% of theoretical values, have been produced using our novel approach. In Table 3.7a, 7b and 3.8a the thickness and mass characteristic of the deposited films are provided. The overall theoretical capacity of Zn/Ag couple is limited by the cathode [33]. In order to increase the achieved capacity and lifetime of our microbatteries, 100% oxidation of the cathode material (Ag) to its highest oxidation number (+2, AgO) needs to be achieved. To make an accurate comparison of our cells achieved capacities with theoretical capacity, we need to make an assumption on the degree of oxidation of Ag in the deposited films. To calculate the maximum theoretical capacity attainable, we assume that all the silver present in the films was oxidized to AgO

(oxidation number +2). Thus the electrochemical equivalent of cathode mass can be calculated based on the following two chemical reactions happening at the cathode during discharge:

$$2AgO + H_2O + 2e^- \rightarrow Ag_2O + 2OH^- \qquad E^0 = +0.607V \qquad (3.1)$$

$$Ag_2O + H_2O + 2e^- \rightarrow 2Ag + 2OH^- \qquad E^0 = +0.342V \qquad (3.2)$$

In theory, for each mol of electrons (e-) lost by the cathode in the discharge reaction, 26.8Ah are produced; thus for each mol of AgO consumed at the cathode, four e- mol are released through reactions (1) and (2), i.e. 107.2Ah. Typically, the theoretical voltage resulting from the two reactions is above 1.7V [32] with lower voltages indicating that only partial reactions are taking place.

anode: Zn (-)

sample	layers	thickness	technique	oxidation time (O_3 atmosphere)
I	Ni/Au/Zn	100Å/500Å/2250Å	PVD	none
II	Cu/Zn	~5000Å (Zn only)	aerosol - spray [1]	none

Table 3.7a: Anode (Zn) deposited films properties [29].

cathode: AgO (+)

sample	layers	thickness	technique	oxidation time (O_3 atmosphere)
I	Ti/Au/Ag	50Å/500Å/1400Å	step 1: PVD step 2: UV oxidation	15 min
II	Ti/Au/Ag	50Å/800Å/1700Å	step 1: PVD step 2: UV oxidation	10 min
III	Ti/Au/Ag	50Å/800Å/1700Å	step 1: PVD step 2: UV oxidation	15 min

Table 3.7b: Cathode (AgO) deposited films properties.

FABRICATED BATTERY PROTOTYPES

Tables 3.8a and 3.8b summarize characteristics and performance of the batteries produced in our study. Calculated theoretical capacities are based on the mass of the cathode only and on the assumption that all the active material (Ag) was oxidized to its highest oxidation number (+2), i.e. AgO. When discharged at high rate (1.4C) the batteries with larger footprint O~cm^2 output a first discharge (formation cycle) capacity ranging 47.5-100μAh. IOS-C-1 2nd cycle capacity was ~25μAh while for IOS-C-3 the 2nd cycle capacity was ~5μAh. When discharged at low rate (C/70), battery IOS-C-2 achieved ~11.25μAh. IOS-M-1 (O~mm^2) achieved a capacity of 2.75μAh in the 1st discharge cycle at 0.7C-rate and 1.25μAh in the 2nd cycle, with a total number of 5 discharge/recharge cycles. IOS-M-2 (O~mm^2) output a capacity of 0.28μAh at low rate (C/150), with no further cycling. The integrated battery IOS-X-1 under variable discharge conditions achieved an overall capacity of 1.1μAh.

battery	Ag area [cm^2]	Ag thickness [nm]	Ag volume [cm^3]	Ag mass [g]	Ag mass [mol]
IOS-C-1	1.2	140	$1.7x10^{-5}$	$1.8x10^{-4}$	$1.7x10^{-6}$
IOS-C-2	1.0	170	$1.7x10^{-5}$	$1.8x10^{-4}$	$1.7x10^{-6}$
IOS-C-3	1.0	170	$1.7x10^{-5}$	$1.8x10^{-4}$	$1.7x10^{-6}$
IOS-M-1	0.010	170	$1.7x10^{-7}$	$1.8x10^{-6}$	$1.7x10^{-8}$
IOS-M-2	0.010	170	$1.7x10^{-7}$	$1.8x10^{-6}$	$1.7x10^{-8}$
IOS-X-1	0.052	140	$7.3x10^{-7}$	$7.7x10^{-6}$	$7.1x10^{-8}$

Table 3.8a: Fabricated batteries: mass and volume of the cathode (limiting electrode).

battery	cathode area [cm²]	cathode mass [mol]	theoretical* capacity	discharge current	C-rate	1st cycle capacity	2nd cycle capacity	number of cycles
IOS-C-1	1.2	$1.7x10^{-6}$	182μAh	250μA	1.4C	100μAh	25μAh	10
IOS-C-2	1.0	$1.7x10^{-6}$	182μAh	2.5μA	C/70	11.25μAh	n/a	n/a
IOS-C-3	1.0	$1.7x10^{-6}$	182μAh	250μA	1.4C	47.5μAh	5.0μAh	10
IOS-M-1	0.020	$3.4x10^{-8}$	3.64μAh	2.5μA	0.7C	2.75μAh	1.25μAh	5
IOS-M-2	0.020	$3.4x10^{-8}$	3.64μAh	25nA	C/150	0.28μAh	n/a	n/a
IOS-X-1	0.052	$7.1x10^{-8}$	7.61μAh	100-200nA	C/70-C/40	1.1μAh	n/a	n/a

* based on cathode mass only , and assuming 100% of Ag is oxidized to AgO

Table 3.8b: Fabricated batteries: characteristics and performance.

BATTERY PACKAGING

Among the batteries produced to complete our study there were few of them that failed to output expected capacities or that did not achieve significant voltages (less than theoretical or failed to recharge). Although we have not included quantitative results from those tests, we would mention them here as a group, and discuss the reasons of failure in the discussion section, as they can provide valuable insight to improve the present prototypes. In several cases electrodes did not properly align and the effective surface area, that could react with the electrolyte, was significantly smaller than expected. Some batteries did not sustain good seals, with resulting electrolyte evaporation or leakage. The third problem manifested was the damage or displacement of the separator membrane with consequent short circuit of the battery.

BATTERY CAPACITY AND LIFETIME

In Figure 3.11 the voltage vs. time profile for battery IOS-C-1, discharged at constant 250μA, is illustrated. The cathode (Ag, limiting electrode) volume, before oxidation, was ~$1.7x10^{-5}cm^3$ with a surface area of $1.2cm^2$ and a thickness of 140nm. The estimated silver (Ag) mass was ~$1.8x10^{-4}$g, i.e. ~$1.7x10^{-6}$mol. The initial output voltage was ~1.5V. The battery was then cycled 10 times with cutoff voltages for discharge and recharge of 0.9V and 1.6V respectively (highlighted in the discharge graph). From the discharge profile (Figure 3.11) we estimated a capacity of approximately 100μAh, resulting from a voltage drop below 0.9V experienced after ~0.4hours in the first cycle. The duration of the second discharge cycle was ~0.1hours and the corresponding capacity was ~25μAh.

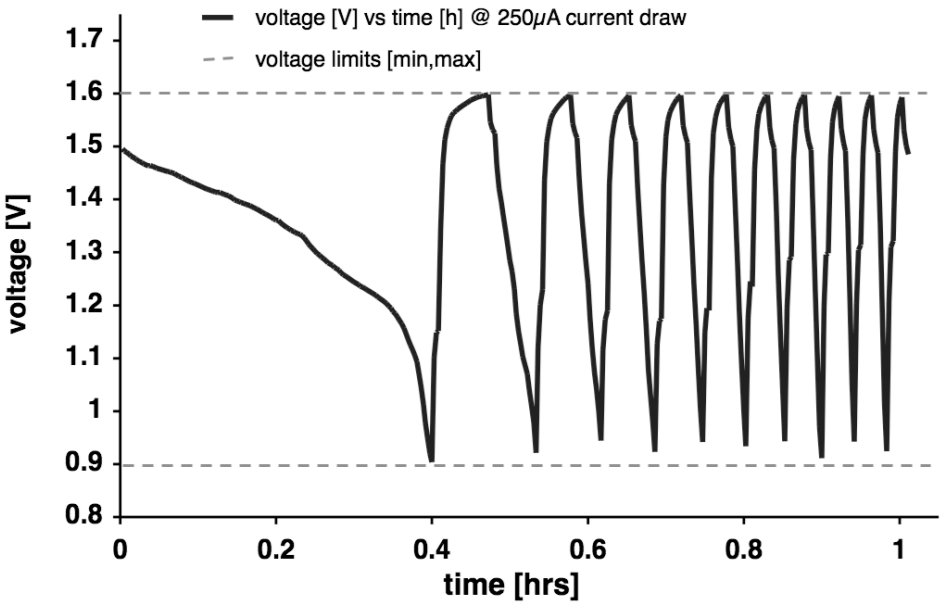

Figure 3.11: IOS-C-1 discharge at 250μA: 10 cycles.

The first discharge cycle of battery IOS-M-1 is depicted in Figure 3.12. The cathode area of the battery was ~$2mm^2$ and the silver mass (170nm thick electrode),

before oxidation, was ~$3.4x10^{-8}$mol. The initial voltage read ~1.55V, which is also the nominal voltage for this chemistry [33]. The battery was discharged at constant 2.5μA for ~1.2hours. Subsequent to the first discharge, the battery was recharged to 1.6V and cycled for five times, at constant 2.5μA, between 0.9V and 1.6V. The voltage versus time plot of the cycle test is reported in Figure 3.13.

Figure 3.16 shows a cycling test conducted on battery IOS-C-3. This battery had an electrode surface area of ~$1cm^2$ with a cathode thickness of 170nm. The volume of silver, before oxidation, was ~$1.7x10^{-5}cm^3$ (same as battery IOS-C-1) with a corresponding mass of ~$1.7x10^{-6}$mol. The battery was discharged at constant 250μA for 10 cycles. In first cycle the 0.9V cutoff was reached after ~11minutes, while in second cycle the cutoff was reached after ~2minutes.

The results of the low rate discharge tests conducted on battery IOS-M-2 and IOS-C-2 are shown in Figure 3.14 and Figure 3.15 respectively. IOS-M-2 had the same geometry and cathode mass of IOS-M-1. For this test, a constant discharge current of 25nA was applied for ~11hours before the cutoff voltage of 0.9V was reached. IOS-C-2 had an electrode area of ~$1cm^2$ and a silver mass (170nm thick electrode), of $1.7x10^{-6}$mol. Discharged at 2.5μA constant current, it reached the 0.9V cutoff voltage after approximately 4.5hours.

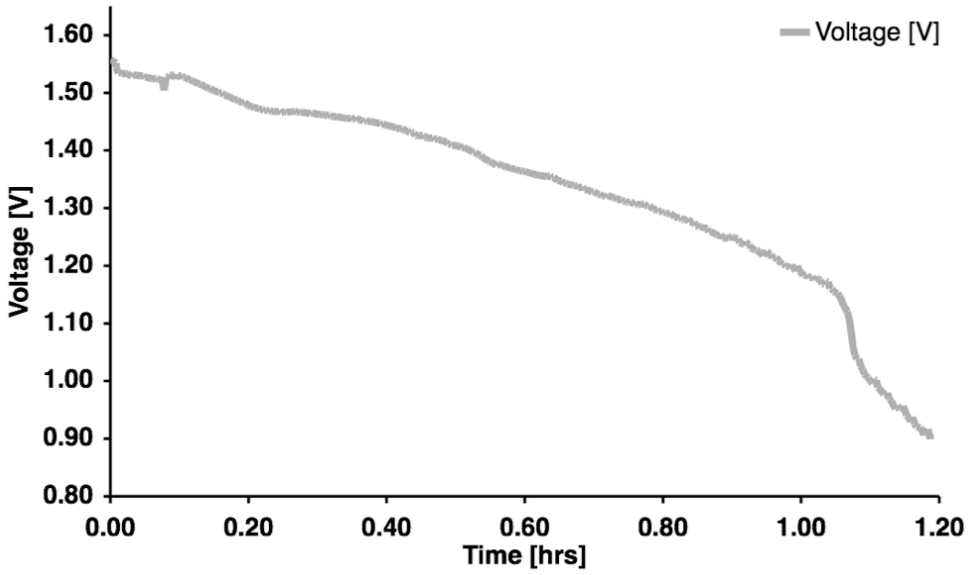

Figure 3.12: IOS-M-1 discharge at 2.5µA: 1st cycle.

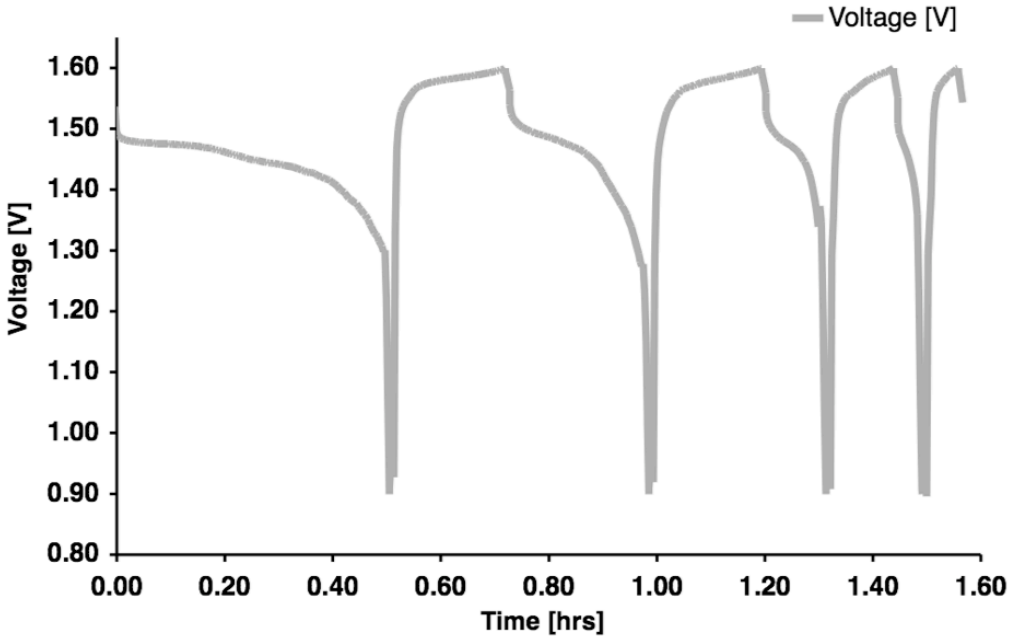

Figure 3.13: IOS-M-1 discharge at 2.5µA: cycles 2nd through 5th.

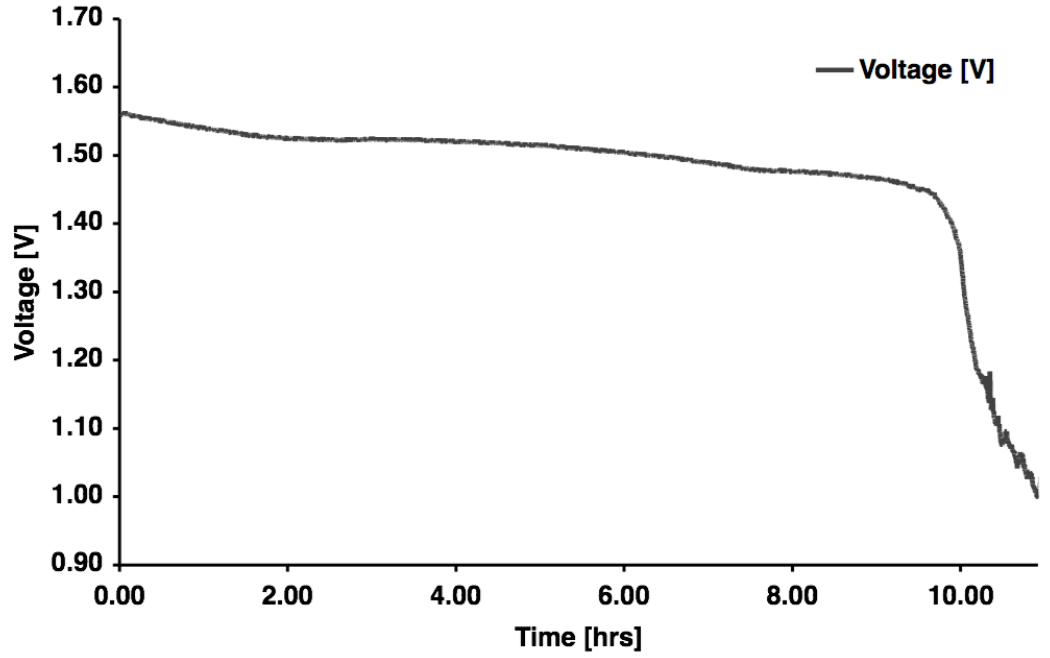

Figure 3.14: IOS-M-2 discharge at 25nA.

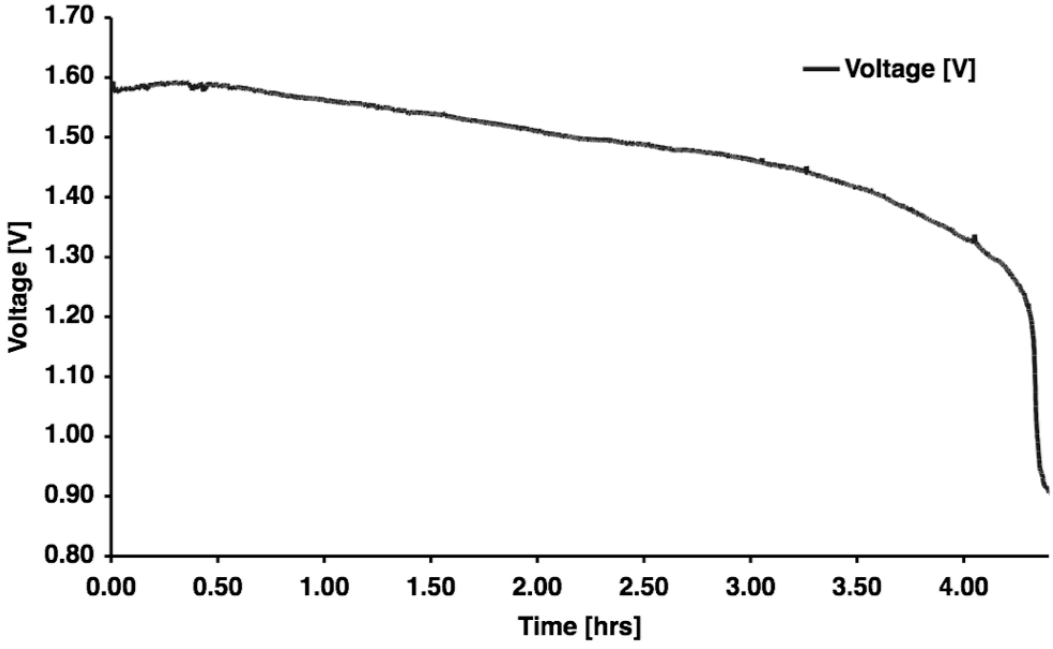

Figure 3.15: IOS-C-2 discharge at 2.5µA.

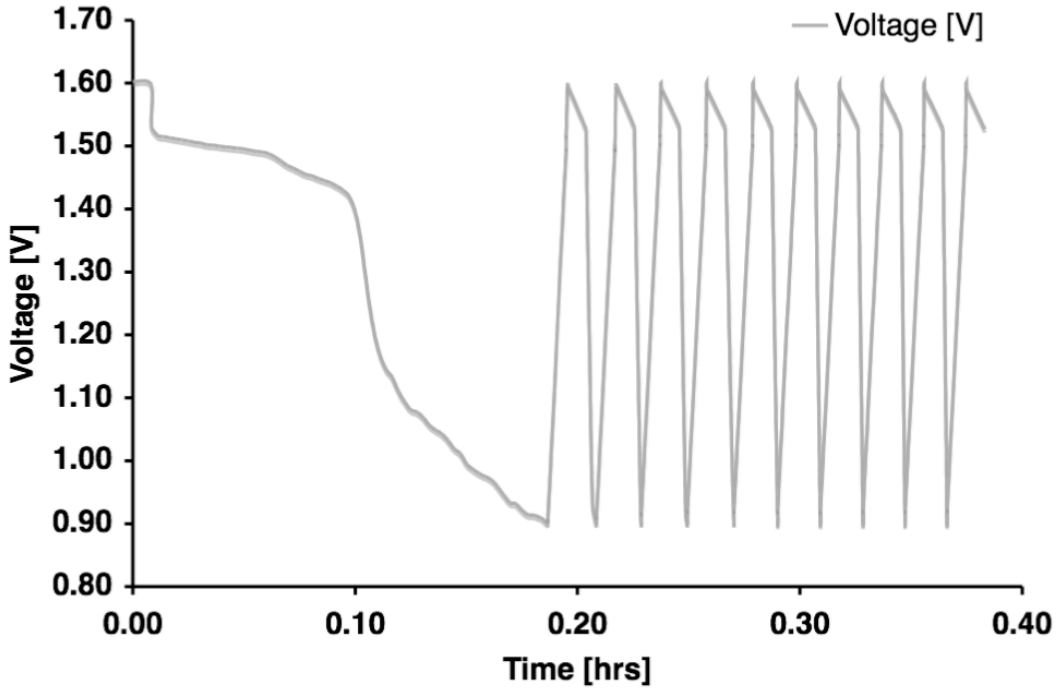

Figure 3.16: IOS-C-3 discharge at 250µA: 10 cycles.

INTEGRATED DEVICE

The discharge voltage and current versus time plots for IOS-X-1 (chip integrated battery) are reported in Figure 3.17 and Figure 3.18 respectively. The first voltage, measured after the battery was sealed, was ~1.6V. The battery was able to power the chip for approximately 9 hours before reaching the 0.9V cutoff voltage. The current draw profile is comprises three steps: 180nA lasting approximately one hour, followed by ~130nA during three hours and ~110nA for 5 hours. The estimated capacity for IOS-X-1 was ~1.1µAh. This cell cathode area was ~5.2mm^2 and the silver volume, prior to oxidation, was ~7.3x10^{-7}cm3 corresponding to a mass of ~7.1x10^{-8}mol.

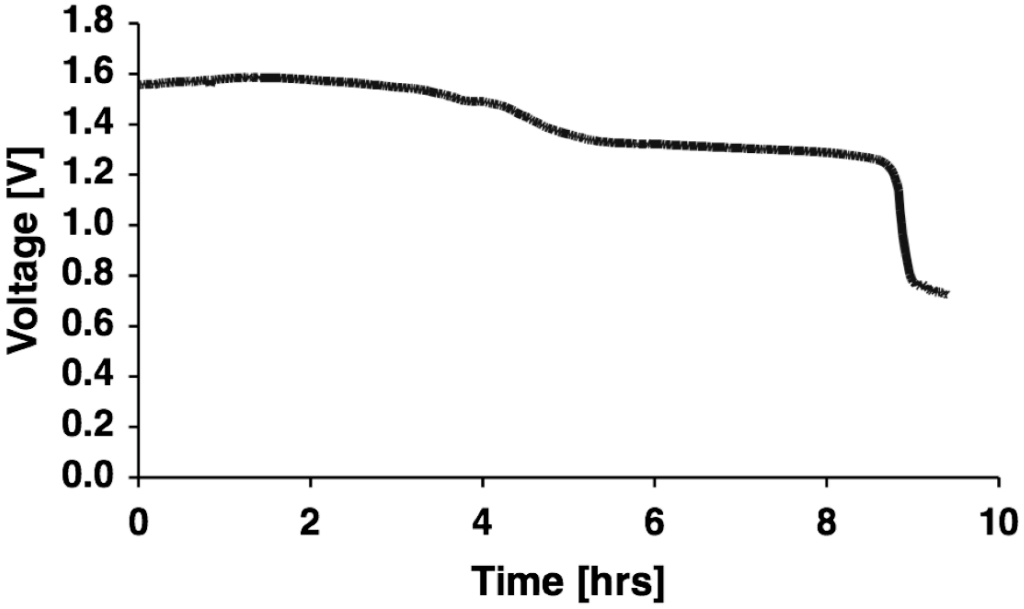

Figure 3.17: IOS-X-1: voltage [V] discharge profile.

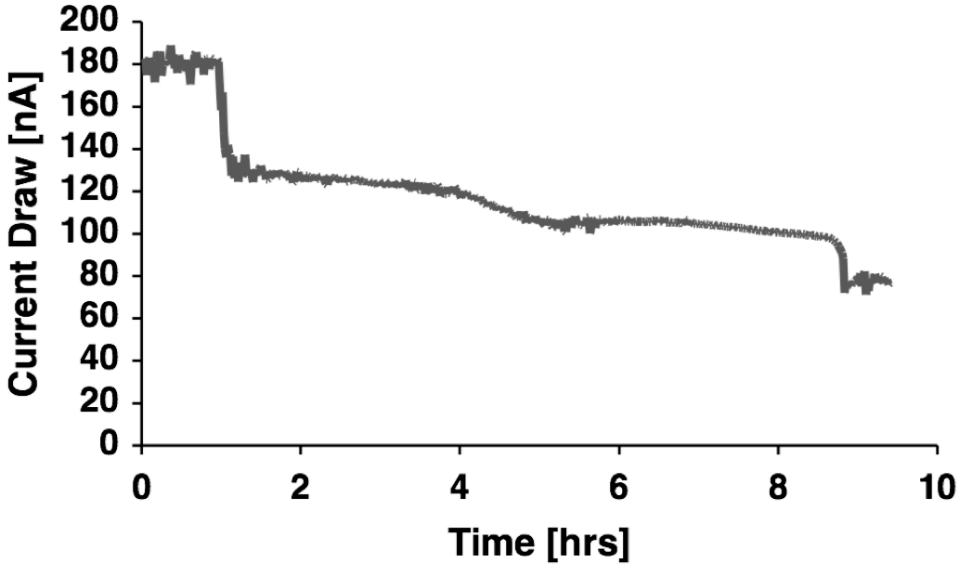

Figure 3.18: IOS-X-1: current [A] discharge profile.

DISCUSSION

COMPARISON TO EARLIER WORK

Inside-the-clean room thin-film battery (TFB) fabrication technologies have been extensively demonstrated, through application of techniques like photolithography [9,15], CVD and sputtering [11], to be effective in miniaturization of PS. However the size reduction introduced using such techniques is only partial. TFBs currently available (Table 3.2) present an intrinsically low capacity that requires large electrode surface areas in order to become useful for MEMS (~30mWh/cm^2 goal [8]). 3D electrodes [19] and microfabrication techniques [20], have been proposed to increase the surface area and get closer to the energy density goal at the same time reducing battery footprint, however the high fabrication cost has been a major limitation. A combination of these two approaches will be needed along with the adoption of cheaper manufacturing technologies to enable optimized power sources for MEMS.

OPTIMUM ELECTROCHEMISTRY

Zn/AgO electrochemistry (Table 3.5) was selected as primary battery candidate based on its high energy density, which allows fabrication of batteries with reduced volumes and masses. The low nominal voltage of this chemistry (1.55V [33]) made it suitable for the present and similar MEMS applications that operate at low power. Among secondary systems a non-commercial $LiCoO_2$ secondary system [11] was proposed. It should be pointed out that this chemistry was never a practical solution for several reasons, first it was a research system (not available); second the only equivalent commercial battery (LS-101 from Infinite Power Solutions [18]), was too large (1x1in^2)

to fit the present geometric constraints; third the lithium (Li) nominal voltage (3.7V) was too high to meet the maximum input voltage (1.6V) of the regulator. Selection of lithium batteries to power low-power MEMS entails energy dissipation (waste), usage of electronics circuitry, cells in special configurations (parallel or in series with resistors) and additional control units. Regulation of 3.7V (optimal for high power applications) to lower levels is therefore an impractical task, resulting in PS with bigger sizes, higher fabrication costs (more steps) and increased complexity (overload of cells, failure mechanisms, hazardous situations will have higher probability to occur).

FABRICATED BATTERIES

The differences between theoretical and experimental capacities across fabricated batteries are likely to be the result of a combination of several factors. First of all the deposited films are not 100% dense, as it is evident from the SEM pictures (Figures 3.7-3.10). In theoretical calculations the electrodes are considered fully dense thus the calculated capacity values are much higher than in real systems.

The second factor, more difficult to quantify, is the uniformity and thickness of the deposited films [34]. The micrograph reported in Figure 3.10, taken after oxidation, shows a non-uniform surface morphology of the cathode. The presence of a rougher surface indicates that the deposited film was probably thinner in that area and allowed higher residual stresses to concentrate and trigger a rougher surface.

Thirdly, the extent of the oxidation, and therefore the amount of active AgO/Ag_2O material in the cathode, directly affects the capacity of the cell and the achieved voltage. The cathode film (limiting electrode) could be made of AgO (+2 oxidation number),

Ag_2O (+1 oxidation number) or a combination of the two, while non-oxidized parts of the cathode would still be made of pure Ag. Longer or shorter oxidation times output different amounts of AgO/Ag_2O. In our theoretical capacity calculations we assumed a cathode made 100% of AgO with a theoretical voltage higher than 1.7V.

IOS-C-1, IOS-C-2 and IOS-C-3 were designed to have all the same cathode volume (Table 3.8a), thus the corresponding cathode mass for each one of them was ~$1.7x10^{-6}$mol. Theoretically, the maximum output capacity of such a cell would be 182μAh (Table 3.8b, 100% AgO cathode). However, several differences among these three batteries could be responsible for their wide variation in performance. First the pure silver (Ag) in the cathode (non oxidized or that is produced during the chemical reaction upon recharge), provides percolated paths that help to keep the internal resistance of the cell low [32]. At the same time, a higher oxidation extent of silver directly affects the capacity of the batteries that is limited by the cathode (AgO). Secondly these three batteries were constructed using cathodes of different thicknesses (Table 3.7b), thus carrying different Ag/AgO content. Normally, graphite is added as an additive to Zn/AgO commercial cells to increase the very poor conductivity of the silver oxide [33]. Our batteries were made without usage of conductive additives, therefore a direct comparison with commercial Zn/AgO batteries cannot be made.

BATTERY PACKAGING

The packaging technique utilized in our study is based only on the mechanical action of Plexiglass clamps utilized to hold the battery electrodes together and the sealing action of a silicone gasket. When the electrodes had millimeter size areas, if the anode

and cathode were not perfectly aligned before the package was sealed, the capacity output was reduced up to 90%, due to less surface area partaking in the chemical reactions. A few batteries were not hermetically sealed and electrolyte evaporation prevented the battery from being recharged. Due to the implantable nature of the sensor this is a particularly critical challenge to address because it directly affects safety and lifetime of the device.

Although this design was effective in granting hermetic seal to the batteries that were successfully discharged, this technique would be unpractical for the final prototype for several reasons. The size of the package would be large and conflict with our miniaturization objective. Direct on-chip integration of the battery would be prevented because of extra packaging processing steps, separated from the electrode deposition. Long-term implantation and FDA approval require a material different than silicone, as it has been shown that it reacts with body fluids and degrades over time [35,36]. Parylene-C films [37] are a suitable alternative packaging material as they deposit, in the gas phase, biocompatible and stress-resistant films that could hermetically seal the deposited electrodes. To prevent leakage during fabrication of a thin-film package, the liquid KOH electrolyte needs to be replaced with a solid or gel material. Long-term seal and leakage of such a package need to be evaluated. Designing a package with the same dimensions (thickness) of the deposited electrodes will reduce size, benefit implantability, and increase specific energy properties of the battery.

BATTERY CAPACITY AND LIFETIME

We demonstrated in this study that the Zn/AgO system could be successfully recharged when the electrodes are manufactured as thin films. The cycling test for IOS-C-1 was run for approximately 1 hour at 1.4C constant rate, produced 10 cycles of discharge/recharge between the voltage of 0.9V and 1.6V. Determination of the battery cycle life (maximum number of cycles) was not a present objective therefore as the cycle duration (time) started to diminish the test was terminated. Similarly IOS-C-3 was discharged at 1.4C for 10 cycles. Both batteries performed better in the first cycle than in the subsequent cycles. The second cycle capacity of IOS-C-1 was only 25% of the first cycle and 10% of the theoretical. For IOS-C-3 the second cycle capacity was ~10% of first cycle and 2% of theoretical. Battery IOS-M-1 had a second cycle capacity ~45% of the first cycle and ~34% of theoretical. The formation cycle (first discharge cycle) is expected to be different from the subsequent cycles [32]. We believe the first discharge outputs higher capacities than the following cycles because, when recharging a cell, Ag does not completely oxidize back to the original AgO (+2 oxidation number), and most of the cathode material is only constituted by Ag_2O (+1 oxidation number) or simply Ag. Cycling the cell at lower rates may provide a way to oxidize the cathode back to the original status. Formation of the SEI layer between the cathode and the electrolyte affects the actual capacity and cycle life of the cell by increasing the cathode resistance, decreasing ionic mobility and conductivity [33,38]. Our thin film batteries were made of pure metals without addition of any conductive additives or performance enhancing particles coatings, thus lower conductivities and faster degradation over cycling are

expected [32]. Our results could be useful to quantify the influence of such additives and coatings to achieve higher capacity or cycle life in commercial systems.

The experimental capacity of IOS-C-1 at 1.4C discharge rate was 100μAh (first cycle, 0.9V cutoff voltage after 0.4h at 250μA discharge current), i.e. ~55% of theoretical. IOS-C-2 was discharged at C/70 rate and the output capacity was 11.25μAh, i.e. only ~6% of theoretical. We believe that the thicker electrode (170nm) and the lower oxidation time (10min) for this battery cathode were responsible for the poor performance compared to IOS-C-1 (see Table 3.7b). The voltage was constant at 1.6V for approximately 1hour (Figure 3.15) and then it experiences a constant negative slope. The change in slope during discharge is related to the exhaustion of the first redox reaction taking place at the cathode (reaction (1) presented above). IOS-C-3 was discharged at 1.4C to verify that the result of IOS-C-1 was reproducible; the output capacity of the first cycle was ~47.5μAh, i.e. ~26% of theoretical. A thicker cathode film than IOS-C-1 and a shorter oxidation time are responsible of this difference (see Table 3.7b).

Battery IOS-M-1 and IOS-M-2 were built with identical cathode volume (Table 3.8a) and they both had a silver mass of ~3.4×10^{-8}mol. Thus the theoretical capacity for such a cell would be 3.64μAh (Table 3.8b). IOS-M-1, discharged at 0.7C, output a capacity of 2.75μAh in the first cycle, i.e. ~76% of theoretical. This very high output is related to the higher content of Ag in this cell compared to others (170nm thick cathode) and its level of oxidation (10 minutes), as a result lower internal resistance and better performance at high rates was achieved. IOS-M-2 was discharged at C/150 (Figure 3.14) and produced 0.28μAh, i.e. ~8% of theoretical. The mostly flat voltage curve for IOS-M-2 and an initial voltage below 1.6V indicate that only the monovalent silver oxide (+1)

specie is predominant for this battery cathode. As a result this battery achieved a lower performance compared to IOS-M-1.

Battery IOS-X-1 achieved a capacity of 1.1μAh ~14% of theoretical. This result is related to the cathode degree of oxidation; the thicker cathode (170nm) and the longer oxidation time (15min) are responsible for it (Table 3.7b). Another factor affecting battery performance is the smaller size of this system compared to IOS-C-1, the corresponding discharge rate being, for the same benchmark, C/10 instead of C/1000. It has been shown how a variable discharge rate can affect the battery performance by more than 50% [39]. In a Zn/Ag system employing 25% KOH as the electrolyte, when the discharge rate is increased from 1C to 2C, the useful capacity of the cell could be limited to 55.6% of its rated capacity [38]. In our system the initial current draw was ~180nA and after one hour dropped to ~130nA (30% reduction) and finally down to ~110nA (40% reduction), the resulting rate changed from C/40 to C/70.

INTEGRATED DEVICE

The integration of the battery with the powered device provides the advantage of a more precise and realistic evaluation of the battery performance by incorporating and accounting for the interaction of multiple factors at the same time. Moreover a realistic device usage with a variable current draw would be difficult to simulate using a battery tester. The effect of such a discharge is shown in Figure 3.17, the flat plateau, typical of the Zn/Ag electrochemistry, was able to accommodate current changes up to 40% during discharge without being affected. The voltage drop presents an inflection point after approximately 5 hours of discharge. This is likely the result of higher oxidation state

cathode material AgO (+2) being exhausted and, at the same time, the onset of lower oxidation state Ag_2O (+1) being consumed. It is unlikely that the variable rate of discharge is responsible for such an inflection point. We believe that the variable rate however is responsible for a shorter-than-theoretical lifetime as supported by similar results of Zn/Ag batteries in the literature [32,38].

Based on the power requirements reported in Table 3.3b, the capacity needed to operate the device would be 100nAh per cycle, totalling 72μAh for 720 cycles (30days, reported in Table 3.3b). In order to achieve such a capacity at 100nA constant draw, $0.67x10^{-6}$mol of AgO would be required, i.e. a cathode volume of ~$0.67x10^{-2}mm^3$. Exploiting all the $3mm^2$ surface area available on the device to deposit a battery, would create a cell with a cathode thickness of ~220μm and a total thickness of ~500μm.

CONCLUSIONS/FUTURE WORK

By modeling the duty cycle of the WIMS-IOS we were able to identify and design an optimized power source [21,22]. The Zn/AgO was the optimum electrochemistry selected for powering the integrated microsystem. When compared with other microfabricated power systems (Table 3.2), Zn/AgO microbatteries have similar energy densities with intrinsically lower power, hence they are the best candidates for MEMS based devices and microsystems.

Direct on-chip fabrication is a key objective for size reduction and integration of the battery, and to realize a fully autonomous and implantable microsystem. We explored the capabilities of novel PVD and aerosol spray technologies to fabricate microbatteries. Outside-the-clean room deposition allowed a low-cost fabrication technique. Remarkable

size reduction introduced by PVD enabled to meet the rigorous volume requirements ($0.42mm^3$) of the IOS; the smallest of our prototypes presented a volume of approximately one third of the available one if we neglect all the bulk packaging with no functionality.

To map capacity and lifetime of the selected electrochemistry, six prototype cells were created and successfully discharged: three O~cm^2 microbatteries (IOS-C-1, IOS-C-2 and IOS-C-3) and three O~mm2 microbatteries (IOS-M-1, IOS-M-2 and IOS-X-1); IOS-X-1 was integrated and directly tested with the device. Cells were fabricated with footprints of $1.2cm^2$ and $1.0cm^2$ for the bigger ones and $2.0mm^2$ and $5.2mm^2$ for the smaller ones (Table 3.8a).

The impedance of silver–zinc cells is normally low, but can vary considerably with factors such as content of silver [32], discharge current, state-of-charge (SoC), cells ageing, operational temperature, separator material and more importantly, cell size [40]. The highest experimental capacity among the bigger cells was 100μAh, achieved by IOS-C-1 at 250μA (1.4C) discharge. Among O~mm^2 cells (Table 3.8b), IOS-M-1 achieved the highest capacity (2.75μAh) at 2.5μA discharge (0.7C rate). Differences among our results are likely to be a consequence of variation of impedance and degree of oxidation among the samples that we utilized to fabricate our batteries.

The effects of microsystem integration and of variable current draw (variable device usage during the day) matched the literature indication that applying a variable discharge rate can affect battery performance by more than 50% [38]. IOS-X-1 achieved a capacity of 1.1μAh (~15% of theoretical) while it was discharged at a variable rate between 100-200nA (imposed by the microchip).

For future work we would like to investigate the statistical significance of factors that affected the performance of microfabricated batteries like electrode thickness, impedance and degree of oxidation. Secondly evaluation of thin-film packaging leakage and seal will be necessary to implement size reduction and evaluate shelf life of our batteries. Thirdly demonstration of a directly on-chip deposited battery is among our goals.

BIBLIOGRAPHY

1. Lemmerhirt, D.F. and Wise, K.D., “Chip-scale integration of data-gathering microsystems,” Proceedings of the Ieee,2006. 94 (6): p. 1138-1159.

2. Sato, H., Berry, C.W., Casey, B.E., Lavella, G., Yao, Y., Maharbiz, M.M., “A Cyborg beetle: insect flight control through an implantable, tetherless microsystem,” accepted 21st IEEE International Conference on Micro Electro Mechanical System (2008).

3. Mohseni, P., Najafi, K., Eliades, S.J., and Wang, X.Q., “Wireless multichannel biopotential recording using an integrated FM telemetry circuit,” Ieee Transactions on Neural Systems and Rehabilitation Engineering,2005. 13 (3): p. 263-271.

4. Nieder, A., “Miniature stereo radio transmitter for simultaneous recording of multiple single-neuron signals from behaving owls,” Journal of Neuroscience Methods,2000. 101 (2): p. 157-164.

5. Johannessen, E.A., Wang, L., Cui, L., Tang, T.B., Ahmadian, M., Astaras, A., Reid, S.W.J., Murray, A.F., Flynn, B.W., Beaumont, S.P., Cumming, D.R.S., and Cooper, J.M., “Implementation of multichannel sensors for remote biomedical measurements in a microsystems format,” Ieee Transactions on Biomedical Engineering,2004. 51 (3): p. 525-535.

6. Obeid, I., Nicolelis, M.A.L., and Wolf, P.D., “A multichannel telemetry system for single unit neural recordings,” Journal of Neuroscience Methods,2004. 133 (1-2): p. 33-38.

7. http://www.plasticlabels.ca/index_files/compareEVbatteries.htm, accessed 12/14/2007.

8. Long, J.W., Dunn, B., Rolison, D.R., and White, H.S., “Three-dimensional battery architectures,” Chemical Reviews,2004. 104 (10): p. 4463-4492.

9. Bates, J.B., Dudney, N.J., Neudecker, B.J., Hart, F.X., Jun, H.P., and Hackney, S.A., “Preferred orientation of polycrystalline LiCoO2 films,” Journal Of The Electrochemical Society,2000. 147 (1): p. 59-70.

10. Bates, J.B., Dudney, N.J., Neudecker, B., Ueda, A., and Evans, C.D., “Thin-film lithium and lithium-ion batteries,” Solid State Ionics,2000. 135 (1-4): p. 33-45.

11. Neudecker, B.J., Dudney, N.J., and Bates, J.B., “"Lithium-free" thin-film battery with in situ plated Li anode,” Journal Of The Electrochemical Society,2000. 147 (2): p. 517-523.

12. Neudecker, B.J., Zuhr, R.A., and Bates, J.B., “Lithium silicon tin oxynitride (LiySiTON): high-performance anode in thin-film lithium-ion batteries for microelectronics,” Journal Of Power Sources,1999. 82 p. 27-32.

13. Dudney, N.J. and Neudecker, B.J., “Solid state thin-film lithium battery systems,” Current Opinion In Solid State & Materials Science,1999. 4 (5): p. 479-482.

14. Bates, J.B., Dudney, N.J., Lubben, D.C., Gruzalski, G.R., Kwak, B.S., Yu, X.H., and Zuhr, R.A., “Thin-Film Rechargeable Lithium Batteries,” Journal Of Power Sources,1995. 54 (1): p. 58-62.

15. Humble, P.H., Harb, J.N., and LaFollette, R., “Microscopic nickel-zinc batteries for use in autonomous microsystems,” Journal Of The Electrochemical Society,2001. 148 (12): p. A1357-A1361.

16. Harb, J.N., LaFollette, R.M., Selfridge, R.H., and Howell, L.L., “Microbatteries for self-sustained hybrid micropower supplies,” Journal Of Power Sources,2002. 104 (1): p. 46-51.

17. LaFollette, R.M., Harb, J.N., and Humble, P., in Sixteenth Annual Battery Conference On Applications And Advances, 2001), p. 349-354.

18. http://www.infinitepowersolutions.com, accessed 06/02/07.

19. Golodnitsky, D., Nathan, M., Yufit, V., Strauss, E., Freedman, K., Burstein, L., Gladkich, A., and Peled, E., “Progress in three-dimensional (3D) Li-ion microbatteries,” Solid State Ionics,2006. 177 (26-32): p. 2811-2819.

20. Wang, C.L., Taherabadi, L., Jia, G.Y., Madou, M., Yeh, Y.T., and Dunn, B., “C-MEMS for the manufacture of 3D microbatteries,” Electrochemical And Solid State Letters,2004. 7 (11): p. A435-A438.

21. Cook, K.A., Albano, F., Nevius, P.E., and Sastry, A.M., “POWER (power optimization for wireless energy requirements): A MATLAB based algorithm for design of hybrid energy systems,” Journal Of Power Sources,2006. 159 (1): p. 758-780.

22. Cook, K.A. and Sastry, A.M., “An algorithm for selection and design of hybrid power supplies for MEMS with a case study of a micro-gas chromatograph system,” Journal Of Power Sources,2005. 140 (1): p. 181-202.

23. Albano, F., Chung, M.D., Blaauw, D., Sylvester, D.M., Wise, K.D., and Sastry, A.M., “Design of an implantable power supply for an intraocular sensor, using POWER (power optimization for wireless energy requirements),” Journal of Power Sources,2007. 170 (1): p. 216-224.

24. Provisional Patent Application No: 60/938232, F. Albano and A.M. Sastry, "Micromachined Deposited Battery," Provisional Application Date: 05/16/2007.

25. Wang, C.W., Sastry, A.M., Striebel, K.A., and Zaghib, K., “Extraction of layerwise conductivities in carbon-enhanced, multilayered LiFePO4 cathodes,” Journal of the Electrochemical Society,2005. 152 (5): p. A1001-A1010.

26. Wang, C.W., Yi, Y.B., Sastry, A.M., Shim, J., and Striebel, K.A., "Particle compression and conductivity in Li-ion anodes with graphite additives," Journal of the Electrochemical Society,2004. 151 (9): p. A1489-A1498.

27. Seok, M., Hanson, S., Lin, Y.-S., Foo, Z., Kim, D., Lee, Y., Liu, N., Sylvester, D.M. and Blaauw, D., "The Phoenix Processor: A 30pW Platform for Sensor Applications," accepted IEEE International Solid State Circuits Conference (2008).

28. Lin, Y.-S., Hanson, S., Albano, F., Tokunaga, C., Haque, R.-U., Wise, K.D., Sastry, A.M., Blaauw, D. and Sylvester, D.M., "Low-Voltage Circuit Design for Widespread Sensing Applications," accepted IEEE International Symposium on Circuits and Systems (2008).

29. http://products3.3m.com/catalog/us/en001/utilities_telecom/electrical_contractors/node_GSGXVSC57Rgs/root_GST1T4S9TCgv/vroot_GSBCDFDZ1Zge/bgel_GSRYBL3GPVbl/gvel_Q2V48VRQDBgl/command_AbcPageHandler/theme_us_electricalcontractors_3_0, accessed 03/27/07.

30. http://www.angstromengineering.com/evolution-vacuum-technology.htm, accessed 03/22/07.

31. http://products.panasonic-industrial.com/datasheets/en/ML414S.pdf, accessed 11/25/2007.

32. http://www.yardney.com, accessed 01/06/2008.

33. Linden, D. and Reddy, T.B., Handbook of Batteries, New York, New York, (2002).

34. Kimoto, M., Yamamoto, Y., and Hirose, K., "Effect of Zirconium(Lv) Chloride on the Oxidation-Reduction Behavior of Silver-Silver Oxide Electrode," Nippon Kagaku Kaishi,1994. (1): p. 18-25.

35. Boateng, S., Lateef, S.S., Crot, C., Motlagh, D., Desai, T., Samarel, A.M., Russell, B., and Hanley, L., "Peptides bound to silicone membranes and 3D microfabrication for cardiac cell culture," Advanced Materials,2002. 14 (6): p. 461.

36. Folch, A. and Toner, M., "Microengineering of cellular interactions," Annual Review of Biomedical Engineering,2000. 2 p. 227.

37. Tunc, M., Cheng, X.H., Ratner, B.D., Meng, E., and Humayun, M., "Reversible thermosensitive glue for retinal implants," Retina-the Journal of Retinal and Vitreous Diseases,2007. 27 p. 938-942.

38. Choi, N.S., Yew, K.H., Kim, H., Kim, S.S., and Choi, W.U., "Surface layer formed on silicon thin-film electrode in lithium bis(oxalato) borate-based electrolyte," Journal of Power Sources,2007. 172 p. 404-409.

39. Venkatraman, M. and Van Zee, J.W., "A model for the silver-zinc battery during high rates of discharge," Journal of Power Sources,2007. 166 (2): p. 537-548.

40. Hariprakash, B., Martha, S.K., and Shukla, A.K., "Galvanostatic non-destructive characterization of alkaline silver-zinc cells," Journal of Power Sources,2003. 117 (1-2): p. 242-248.

41. http://www.wimserc.org, accessed October 24th 2005, Amadeus Cochlear Implant (conceptual device).

42. http://www.northstarneuro.com, accessed October 24th 2005, neurostimulator.

43. http://www.wimserc.org, accessed July 2005, intraocular testbed (conceptual device).

44. modified without permission from: http: // www.angstromengineering.com / evolution-vacuum-technology.htm, accessed 04/10/07.

45. Cardenas-Valencia, A.M., Dlutowski, J., Knighton, S., Biver, C.J., Bumgarner, J., and Langebrake, L., "Aluminum-anode, silicon-based micro-cells for powering expendable MEMS and lab-on-a-chip devices," Sensors And Actuators B-Chemical,2007. 122 (1): p. 328-336.

46. Navone, C., Pereira-Ramos, J.P., Baddour-Hadjean, R., and Salot, R., "High-capacity crystalline V2O5 thick films prepared by RF sputtering as positive electrodes for rechargeable lithium microbatteries," Journal Of The Electrochemical Society,2006. 153 (12): p. A2287-A2293.

47. Kushida, K., Kuriyama, K., and Nozaki, T., "Hundred-micron-sized all-solid-state Li secondary battery arrays embedded in a Si substrate," Applied Physics Letters,2002. 81 (26): p. 5066-5068.

48. Jones, S.D. and Akridge, J.R., "Development And Performance Of A Rechargeable Thin-Film Solid-State Microbattery," Journal Of Power Sources,1995. 54 (1): p. 63-67.

49. http://www.telemrk.com/telemrk/cat_evapguide.htm, accessed 03/27/07.

CHAPTER IV

CONCLUSION

SUMMARY

In our study we fabricated high-tech thin-film micro- batteries, outside-the-clean room, to specifically respond to the increasing demand of low-cost, small-size and low-power applications like the WIMS-ERC testbeds and other commonly used devices, e.g. cellphones, PDA's, mp3 players, digital cameras, implantable medical devices and environmental sensors (defense) [1].

A novel method, based on physical vapor deposition (PVD) and aerosol spray, was designed and implemented to build thin-film batteries of microscopic footprints, outside-the-clean room at low temperature and potentially low cost. The method uses a vacuum chamber with a pressure of the order of 10^{-7} Torr and evaporation boats resistively heated to reach the melting temperatures of the metal particles deposited as thin films. This method enables evaporation of metals at temperatures between 270ºC and 500ºC (1/2 to 2/3 of the melting point) creating a vapor that can be directly deposited onto MEMS substrates and packaging. It also allows a large variety of materials to be deposited, including pure metals, ceramic compounds and polymers. Our methodology

represents a novel approach to fabricate thin-film micro- batteries and a valuable alternative to the current clean-room processes used to fabricate thin-film batteries.

Using our method we built thin-film Zn/AgO microbatteries and we thoroughly compared them with current thin-film batteries that utilize 3-D electrodes architectures [2] and C-MEMS structure [3] and past thin-film batteries [4, 5] built using inside-the-clean room manufacturing processes. The processing conditions of our method are significantly different than both photolithography processing and C-MEMS manufacturing as the process takes place at room atmosphere and without usage of any masking or chemical etchant. Also the micro-structural and compositional analyses show that PVD deposition gives thinner electrodes ($\leq 1\mu m$), a more porous structure and a similar composition of other reported thin film technologies. Nonetheless the energy density (40Wh/L) and specific capacity ($100\mu Ah/cm^2$) of our batteries are similar to the other thin-film batteries reported in the literature. This comparison further verified that PVD and spray deposition should be considered as a valuable addition to the current thin-film battery fabrication technologies.

Uneven surface morphology was discovered in the PVD deposited silver (Ag) films, believed to be an evidence of non-uniform film thickness distribution and stress concentration. Surface patterns and ridges formed after the films were exposed to oxidating atmosphere (O_3) for times longer than 10 minutes. We believe the driving force for this surface morphology is the release of residual stresses in the thin film coupled with differences in the film thickness. The zinc (Zn) films, as produced using spray deposition, revealed a highly porous structure with pore sizes up to few μm, believed to

be beneficial to capture electrolyte and facilitate chemical reaction during battery discharge.

Voltage curves resulting from the discharge experiments were analyzed and discussed in terms of capacity. A total of nine prototype batteries were produced and tested with sizes ranging from $1mm^2$ to few cm^2 and capacity up to $100\mu Ah/cm^2$. Capacities up to 75% of the expected theoretical values were observed. Our fabricated micro- batteries fall within the energy density limits of commercial thin-film storage systems ($100\mu Ah/cm^2$ [6]) and two orders of magnitude below the MEMS energy goal ($20mAh/cm^2$ [7]).

The evolution of experimental capacity with cathode composition (limiting electrode) was investigated and compared to theoretical capacity. The effect of oxidation extent in silver (Ag) films was investigated by testing two different oxidation times 10min and 15min and oxidizing two different electrodes thicknesses 140nm and 170nm. The results indicated that the produced cathodes were not fully oxidized, as the output voltage of these batteries was at the most 1.6V. Theoretically for a fully oxidized silver (Ag) cathode (100% AgO) the output voltage vs zinc (Zn) is expected to be 1.76V. In spite of the fact that the lack of oxidation resulted detrimental for the battery capacity, it was found to be beneficial in the reduction of cathode internal resistance. We believe that percolating paths of unoxidized silver act as conventional conductive additives (graphite) in macroscopic silver-oxide cathodes, thus they facilitate electron migration and enhance the overall performance of our batteries.

The effects of integration and variable discharge schedule were evaluated for one of the battery prototypes by testing the system *in-situ* while powering the WIMS-IOS

microchip. We found out that the influence of a variable discharge schedule affects the battery lifetime and capacity as suggested in the literature, however the full battery-device integration presented here represents a first and was enabled by the proposed fabrication technique to produce microbatteries of sub-millimeter footprints. The focus for improving microbatteries has mainly been on increasing the capacity by producing high-surface area electrodes with very exotic shapes and microstructures and investigating new cathodes, electrolytes and conductive additives. This has not been a huge success due to the high costs of clean-room manufacturing, the high costs of new materials and low capacity and conductivity of produced films. Thus large surface areas were needed to build electrodes using previously reported techniques, carrying high costs and creating large battery footprints that prevented integration in portable electronics and MEMS devices.

The author suggests that instead of focusing solely on the microstructure of the cathode and the materials properties like capacity and conductivity, the focus should be on the device as a whole including the battery as one of the elements to be optimized. Hence size reduction, cost of processing and compatibility of the processing conditions with MEMS materials should be all factors that considered at the same time and not individually.

FUTURE WORK

Packaging is the most important limitation of the present prototypes. Modification of the apparatus for PVD deposition would be of great value to enable packaging at the same time of manufacturing. This could be done for example by adding a second

deposition chamber, with the same vacuum atmosphere of the first one, to deposit polymer films after the electrodes are completed. As the selected testbed (WIMS-IOS) represents an implantable application, a perfect seal of the battery is imperative for FDA approval. Evaluation of package hermeticity and shelf life requires long term testing that was not performed in our study. Moreover in order to achieve on-die battery fabrication at the same time of the device assembly, thin film packaging materials (parylene) need to be explored and their seal and leakage quantified. Improving the packaging of thin film batteries will also benefit the goals of size reduction, energy density increase, device integration and implantability.

Testing other electrochemistries (e.g. lithium) fabricated using the same PVD technique validated for fabricating silver (Ag) electrodes is a future goal. Deposition of other metals, alloys and ceramic compounds can be demonstrated using the same vacuum evaporation chamber. Pure lithium (Li) metal requires special care to prevent reaction by contact with moisture, hence the employment of a glove box is necessary to handle this kind of electrodes. The effects of using solid-state electrolyte to build thin-film lithium batteries should be explored by characterizing the transport properties (diffusion coefficient, ionic and electronic conductivity) of electrolyte films and interface phenomena between electrodes and electrolyte (Solid-Electrolite Interface (SEI) layer).

Cost has been a major impediment for application of thin-film batteries technologies in energy storage systems. We presently estimated our battery costs in 6$/Wh based on the amount of raw materials (~1.8×10^{-4} g of Ag) utilized to fabricate a battery of 100µAh capacity. However our method requires in average ~1.5g of material to deposit a ~700Å thick film. The electrodes we fabricated were approximately double

this thickness and ~3g of material were used in the deposition. Thus in order to minimize the waste of material and for this price estimate to be correct, at least 16,000 batteries need to be produced in one deposition. Equipment costs are not included in this estimate as they represent indirect costs, however the investment of a clean room facility is approximately $50M [8], i.e. two orders of magnitudes higher than that of the utilized manufacturing apparatus. In the future increasing quantity of produced battery could reduce the cost of the final product and bring it closer to more conventional commodity batteries.

BIBLIOGRAPHY

1. http://www.insidedsp.com/Articles/tabid/64/articleType/ArticleView/articleId/113/Inside-DSP-on-Low-Power-Long-Live-the-Battery.aspx, accessed 01/13/2008.

2. Golodnitsky, D., Yufit, V., Nathan, M., Shechtman, I., Ripenbein, T., Strauss, E., Menkin, S. and Peled, E., "Advanced materials for the 3D microbattery," Journal of Power Sources, 2006. 153 (2): p. 281-287.

3. Wang, C.L., Taherabadi, L., Jia, G.Y., Madou, M., Yeh, Y.T. and Dunn, B., "C-MEMS for the manufacture of 3D microbatteries," Electrochemical and Solid State Letters, 2004. 7 (11): p. A435-A438.

4. Bates, B., Dudney, N.J., Neudecker, B., Ueda, A. and Evans, C.D., "Thin-film lithium and lithium-ion batteries," Solid State Ionics, 2000. 135 (1-4): p. 33.

5. Humble, P.H., Harb, J.N. and LaFollette, R., "Microscopic nickel-zinc batteries for use in autonomous Microsystems," Journal Of The Electrochemical Society, 2001. 148 (12): p. A1357.

6. http://www.infinitepowersolutions.com, accessed 06/02/2007.

7. Long, J.W., Dunn, B., Rolison, D.R. and White, H.S., "Three-dimensional battery architectures," Chemical Reviews, 2004. 104 (10): p. 4463-4492.

8. Guo, L.J., "Recent progress in nanoimprint technology and its applications," Journal of Physics D: Applied Physics, 2004. 37: p. R123–R141.